Vol. 36 • No. 43 • October 24 • 2024

www.advmat.de

ADVANCED MATERIALS

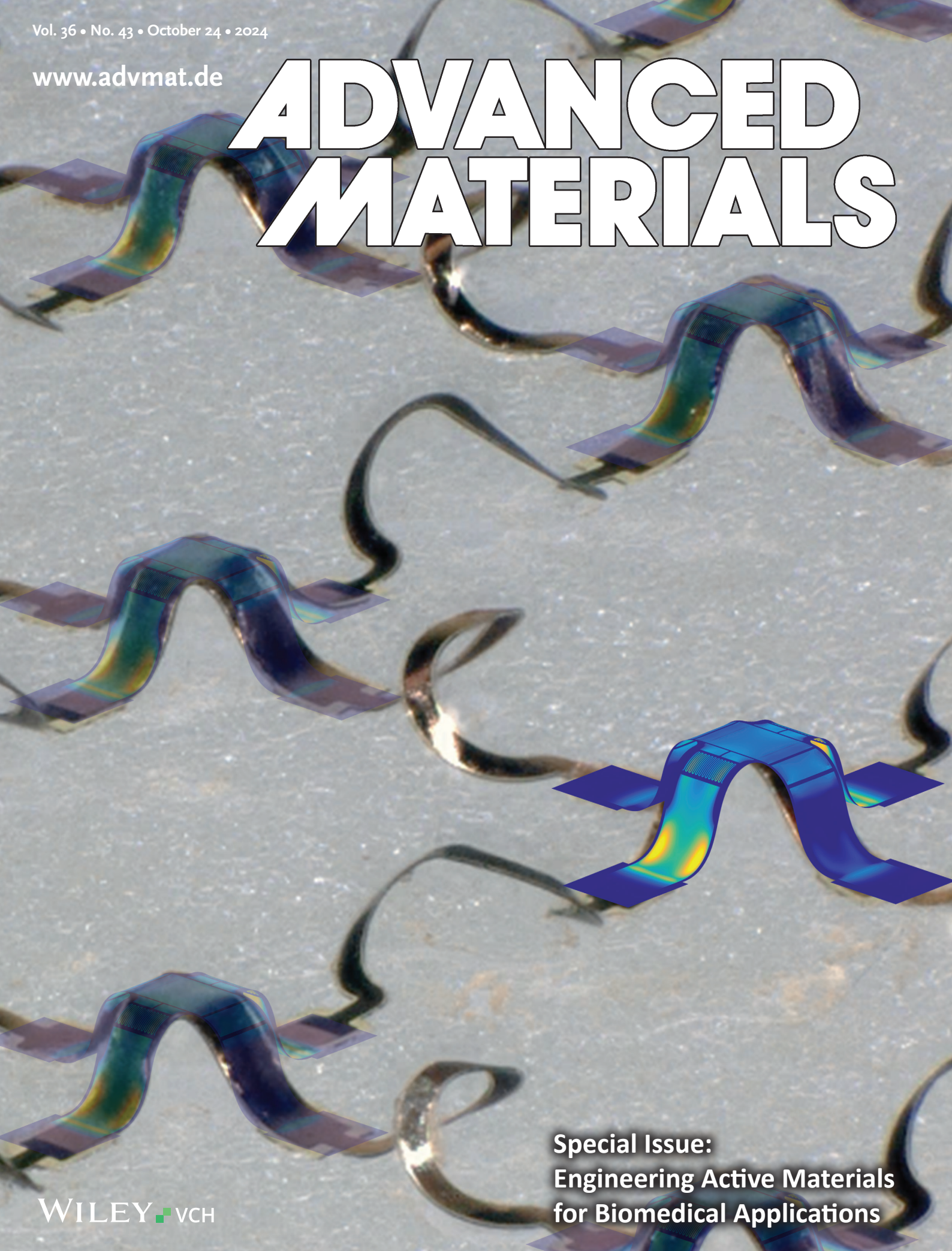

Special Issue:
Engineering Active Materials
for Biomedical Applications

WILEY VCH

ADVANCED MATERIALS
www.advmat.de

Mechanically Active Materials and Devices for Bio-Interfaced Pressure Sensors—A Review

Zhongyi Nie, Jean Won Kwak, Mengdi Han, and John A. Rogers**

Pressures generated by external forces or by internal body processes represent parameters of critical importance in diagnosing physiological health and in anticipating injuries. Examples span intracranial hypertension from traumatic brain injuries, high blood pressure from poor diet, pressure-induced skin ulcers from immobility, and edema from congestive heart failure. Pressures measured on the soft surfaces of vital organs or within internal cavities of the body can provide essential insights into patient status and progression. Challenges lie in the development of high-performance pressure sensors that can softly interface with biological tissues to enable safe monitoring for extended periods of time. This review focuses on recent advances in mechanically active materials and structural designs for classes of soft pressure sensors that have proven uses in these contexts. The discussions include applications of such sensors as implantable and wearable systems, with various unique capabilities in wireless continuous monitoring, minimally invasive deployment, natural degradation in biofluids, and/or multiplexed spatiotemporal mapping. A concluding section summarizes challenges and future opportunities for this growing field of materials and biomedical research.

Z. Nie, M. Han
Department of Biomedical Engineering
College of Future Technology
Peking University
Beijing 100871, China
E-mail: hmd@pku.edu.cn
J. W. Kwak, J. A. Rogers
Querrey Simpson Institute for Bioelectronics
Northwestern University
Evanston, IL 60208, USA
E-mail: jrogers@northwestern.edu
J. W. Kwak, J. A. Rogers
Department of Mechanical Engineering
Northwestern University
Evanston, IL 60208, USA
J. A. Rogers
Departments of Biomedical Engineering
Materials Science and Engineering
Neurological Surgery
Chemistry
and Electrical Engineering and Computer Science
Northwestern University
Evanston, IL 60208, USA
The ORCID identification number(s) for the author(s) of this article can be found under https://doi.org/10.1002/adma.202205609.

© 2023 The Authors. Advanced Materials published by Wiley-VCH GmbH. This is an open access article under the terms of the Creative Commons Attribution License, which permits use, distribution and reproduction in any medium, provided the original work is properly cited.

DOI: 10.1002/adma.202205609

1. Introduction

The human body responds to pressures that naturally occur inside the body (e.g., intraocular pressure, IOP; intracranial pressure, ICP; blood pressure, BP) or to those that follow from external forces. In extreme cases, these pressures can damage essential tissues and initiate a cascade of adverse responses, such as those associated with brain injuries,[1,2] ocular hypertension,[3–6] cardiovascular diseases,[7–11] and skin ulcers[12–14] (**Figure 1**A). Monitoring of pressures applied to soft biological tissues demand sensors that are compatible with their mechanical properties and curved shapes,[15] to enable accurate measurements without irritation. Emerging design strategies for such types of pressure sensors overcome the disadvantages of conventional devices (i.e., the rigid, bulky, and stiff form factors) by exploiting advances in: i) mechanically active materials (i.e., materials that convert mechanical input to changes of material properties or vice versa[16,17]) that respond to strains through resistive, capacitive, piezoelectric, and/or triboelectric mechanisms (Figure 1B); ii) structural designs that exploit 3D geometries, micropatterns, meshes/fibers, and cavities (Figure 1C); iii) system properties that render soft mechanical properties and shape-matched geometries, in array configurations for spatiotemporal mapping, in miniaturized layouts for minimally invasive deployment, and/or in bioresorbable embodiments for use as temporary implants (Figure 1D).

This review focuses on progress in these classes of bio-interfaced pressure sensors, with an emphasis on properties of mechanically active materials, design considerations for biomedical applications, system-level engineering aspects and pre-clinical trials (i.e., noninvasive pressure sensors deployed on patients, and invasive sensors implanted in animal models). Other reviews focus mainly on device mechanisms and supporting electronics,[18–27] in a general sense. An important goal in the following is to highlight developments in the service of specific biomedical applications of pressure sensors for soft tissues. The orientation is around unusual approaches in materials science, mechanical engineering and biomedical engineering. For bio-interfaced pressure sensors with different mechanisms, materials, and structures, this review discusses the performance metrics and properties of pressure sensors for

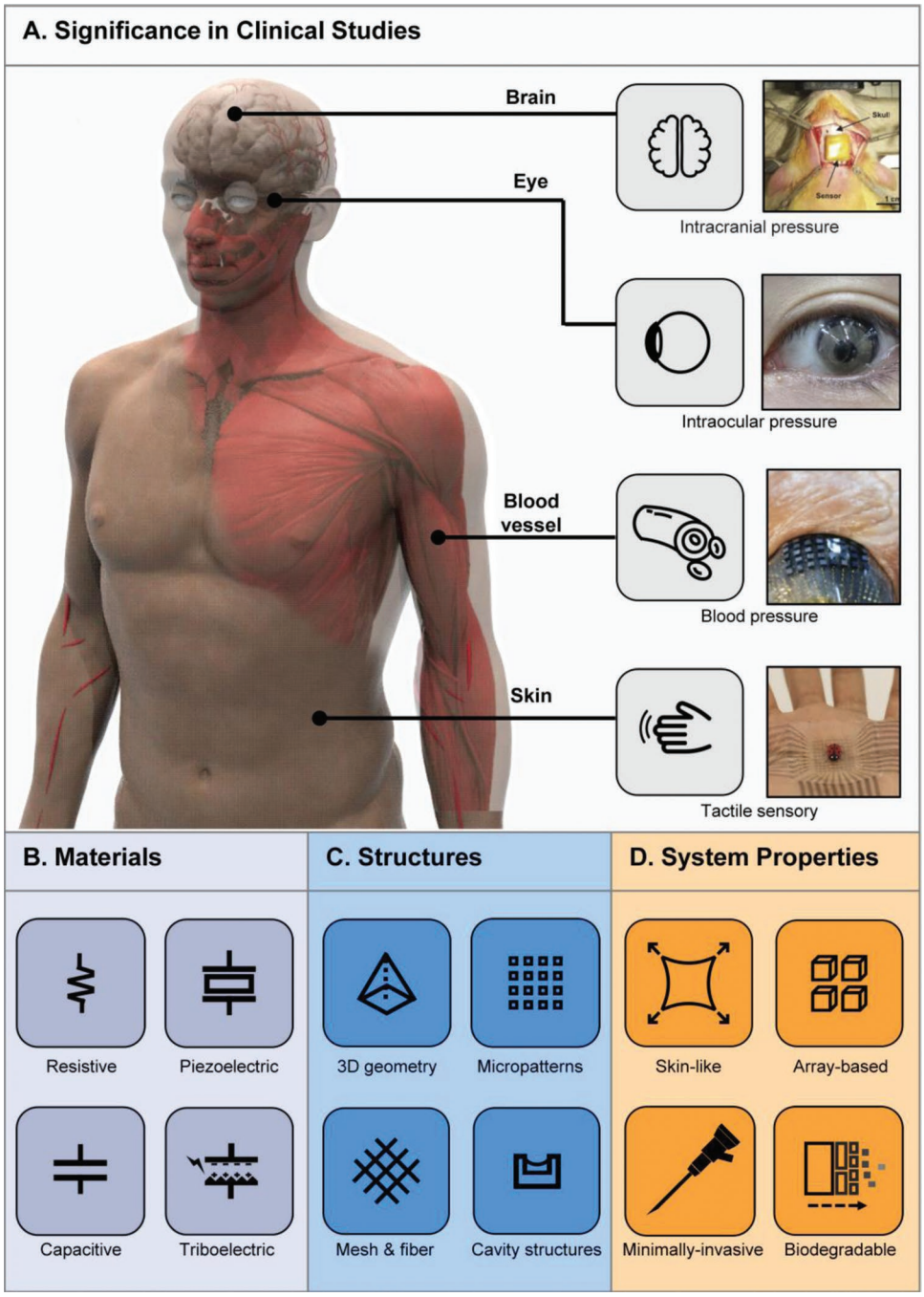

Figure 1. Bio-interfaced pressure sensors. A) Clinical applications of bio-interfaced pressure sensors. Reproduced with permission.[6,7,15,245] Copyright 2020, Wiley-VCH; Copyright 2018, 2020, 2021, Springer Nature. B) Materials for bio-interfaced pressure sensors. C) Structures for bio-interfaced pressure sensors. D) System properties for bio-interfaced pressure sensors.

accurate and stable operation in specific biomedical scenarios, including measurements of BP, ICP, pressures at the skin interface, and others. The content includes manufacturing approaches, materials choices, geometrical configurations, integration with wireless platforms, and progress in clinical translation. A concluding section summarizes the status of the field and lists areas of opportunity for continued research in this area.

2. Metrics, Mechanisms, and Structures for Bio-Interfaced Pressure Sensors

Bio-interfaced pressure sensors must possess physical properties and shapes compatible with those of targeted points of integration with the body. High linearity, fast response time, low drift and hysteresis, and long-term stability are also important considerations. This section focuses on metrics, design

© 2023 The Authors. Advanced Materials published by Wiley-VCH GmbH

RIGHTSLINK

15214095, 2024, 43, Downloaded from https://onlinelibrary.wiley.com/doi/10.1002/adma.202205609 by Northwestern University Libraries, Wiley Online Library on [25/10/2024]. See the Terms and Conditions (https://onlinelibrary.wiley.com/terms-and-conditions) on Wiley Online Library for rules of use; OA articles are governed by the applicable Creative Commons License

15214095, 2024, 43, Downloaded from https://onlinelibrary.wiley.com/doi/10.1002/adma.202205609 by Northwestern University Libraries, Wiley Online Library on [25/10/2024]. See the Terms and Conditions (https://onlinelibrary.wiley.com/terms-and-conditions) on Wiley Online Library for rules of use; OA articles are governed by the applicable Creative Commons License

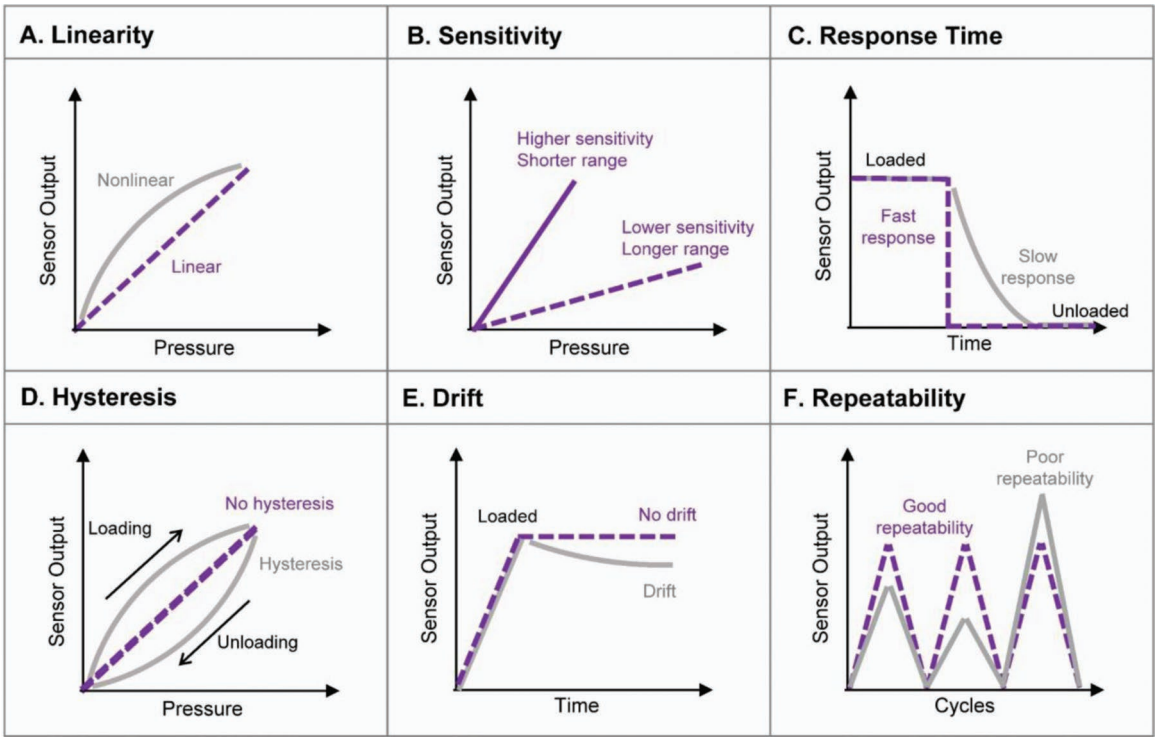

Figure 2. Performance metrics for pressure sensors. A) Linearity. B) Sensitivity and linear response range. C) Response time. D) Hysteresis. E) Drift. F) Repeatability.

considerations, and associated mechanisms for various functional materials and structures that meet many of the key requirements.

2.1. Metrics

Figure 2 summarizes important parameters that define the performance of pressure sensors, including, linearity (Figure 2A), sensitivity and dynamic range (Figure 2B), response time (Figure 2C), hysteresis (Figure 2D), drift (Figure 2E), and repeatability (Figure 2F).

Linear response facilitates calibration procedures by reducing fitting equations to first-order polynomials (purple curve in Figure 2B). In linear regression models, the coefficient of determination (R^2, ranges between 0 and 1) quantitatively defines linearity, where larger R^2 corresponds to better linear response. By contrast, nonlinear responses (grey curve in Figure 2B) require complex computational analysis, sometimes in the form of segmented linear equations.[28–30] In these cases, calibrated pressures that lie between two segmented lines can exhibit discrepancies that may misinform clinical decisions (e.g., improper drug dosages for hypertension). To approximate a linear response, conventional pressure sensors adopt small deflections/deformations of responsive materials or structures, to yield R^2 values that can approach 1.[31–33] Because bio-interfaced pressure sensors incorporate materials and designs with low stiffnesses, applied pressures can produce large displacements/deformations and associated nonlinearities. Structural designs that limit these large deformations are therefore often necessary.

Most pressure sensors can operate linearly only across a limited range (i.e., linear response range, or dynamic range). This parameter relates to and is often balanced with sensitivity (slopes of the curves shown in Figure 2B), according to application requirements, where high sensitivity usually results in a small linear response range. This tradeoff between sensitivity and linear response range must be considered in the design of pressure sensors to match specific applications. For example, the targeted pressure ranges are: i) 0–300 mmHg (0–40 kPa[34]) for BP (below 60 mmHg (diastolic)/90 mmHg (systolic) indicates hypotension and above 90 mmHg (diastolic)/140 mmHg (systolic)[35] indicates hypertension); ii) from 0 to 70 mmHg (0 to 9.33 kPa)[36] for ICP (above 20–25 mmHg indicates intracranial hypertension[37]); iii) 10 to 100 mmHg (1.33 to 13.33 kPa[38]) for IOP (above 21 mmHg indicates ocular hypertension[39]). In other biomedical applications, sensors must record the contact pressures between skin and external objects. Here, the pressure values can vary by more than an order of magnitude. For example, finger grip manipulation requires high sensitivity over a small range from 1 to 10 kPa.[40] In comparison, pressure measurements at the interface between the skin and the inner surface of a prosthetic socket for a load-bearing part of a lower limb demand measurements of pressures up to values of 350 kPa.[12] Optimizing the structures and the materials for bio-interfaced pressure sensors represent two major strategies for adjusting the sensitivity and linear response range. Structures with low stiffnesses usually yield high sensitivity and small linear response range.[41,42] The development of soft materials with large gauge factors (GFs, defined as the ratio of relative change in resistance to the mechanical strain), high dielectric

© 2023 The Authors. Advanced Materials published by Wiley-VCH GmbH

constants or large piezoelectric coefficients, as examples, can improve the sensitivity without reducing the linear response range.[43,44]

Response time is another important metric, typically defined as the time for a sensor to achieve 63.2% of its final reading after application of pressure.[45,46] This time is important for characterizing dynamic variations in pressure, such as those associated with BP or physical activity. Materials and mechanical considerations can influence the response time. For example, silicon pressure sensors that exploit cavity designs usually exhibit very fast responses (<0.1 ms).[47] In comparison, certain sensors based on low modulus elastomers offer slow responses (>10 ms)[48] due to the viscoelastic properties of the materials. As a practical matter, achieving response times that exceed those associated with most natural biological processes and those involved in health-related applications is not difficult (≈1 s for BP cycle and ≈0.6 s for plantar pressure cycle when running). Bio-interfaced pressure sensors for many applications adopt low modulus materials or viscoelastomers to allow for soft and conformal contact without meaningful reductions in response time.

Stress relaxation in such types of soft materials can, however, introduce hysteresis and drift[49] effects that significantly degrade the performance. Mechanical hysteresis, defined by the extent to which the response of the sensor depends on the time history of loading or unloading, directly affects the accuracy. In Figure 2A, the grey and purple curves illustrate pressure sensors with and without hysteresis, respectively. Elastic materials (e.g., metals) obey Hooke's law and possess identical loading and unloading paths, as the stress and strain are linearly related. By contrast, viscoelastic materials exhibit stress-strain behaviors consistent with internal dissipative mechanisms that lead to different loading paths depending on the history of mechanical deformations of the sample, including rate, amplitude and temperature.[50] The practical significance of this hysteresis on the performance of the sensor can depend on the thicknesses and structures of the materials.[51] Engineering considerations in the device layouts can, therefore, be selected to minimize these effects. Approaches to mitigate hysteresis include constraining the compressive strains in the elastomers (e.g., the response of polydimethylsiloxane (PDMS) at compressive strains less than 15% shows negligible hysteresis),[52] incorporating nanocrack morphologies,[53] and integrating micropatterns to the elastomers.[51,53,54]

Drift is the change in sensor responses over time, also relevant to accuracy, particularly for applications such as those in monitoring pressure-induced injuries, where pressures remain at significant and largely static levels over long periods of time (Figure 2E). For viscoelastic materials, stress relaxation or creep is an intrinsic property where the strain increases under constant stress. This change, when it occurs in the sensitive element of a sensor or in some essential structural element, results in drift.[55] In addition to applications in pressure injuries, drift is important in measurements of ICP and IOP, where the pressures change slowly in time. In such situations, sensors must be designed to avoid large strains in viscoelastic materials. Minimizing the influence of temperature, humidity, and other environmental factors is also important.[56] Strategies include the use of materials that have low temperature coefficients of response (i.e., alloys instead of pure metals)[7] and of compliant encapsulating structures that insulate the sensor from the surrounding environment.[36]

Repeatability is important for robust, stable operation, of particular importance for chronic measurements. As an example, patients with hypertension require long-term management to prevent acute cardiovascular diseases, in which case the repeatability of pressure sensors is of vital importance. Applying multiple cycles of loading and unloading to a sensor represents the most common means for quantifying repeatability (Figure 2F). In the elastic response regime, materials typically show good stability.[57] Irreversible changes associated with mechanical failure due to fracture or plastic deformation represents the most obvious sources of poor repeatability. Fatigue – a phenomenon where a material gradually fails when subjected to many cycles of loading/unloading – is an important factor. In-depth understanding of the properties of the constituent materials of a sensor, including but not limited to the maximum strain in the elastic region, the physical toughness, the threshold for plastic yielding and effects of internal flaws, is important. Designing certain structures or geometries to avoid plastic deformation (e.g., <0.3% for metals, <10% for Si nanowires[58]) during operation is essential. For bio-interfaced pressure sensors that mainly incorporate soft materials, combining materials with different moduli (e.g., 1.3 and 5.1 MPa[59]) results in heterogenous distributions of strain (i.e., lower strain in higher modulus parts) that can be designed to avoid plastic deformations or fatigue.[59]

Other considerations, such as those related to interference, power consumption, cost, and mass production are also important. Confounding effects related to changes in temperature, humidity, parasitic capacitances and other externalities are particularly important for biomedical applications in critical care and decision making that depend on accurate measurements.[45] Low power or self-powered systems can affect form factors by relaxing or eliminating requirements for batteries or for power transfer from external sources.[60–62] Cost effective, volume production is also important, particularly because many medical uses are addressed most effectively with single-use devices to avoid the need for cleaning and sterilization.

2.2. Mechanisms and Materials for Different Types of Pressure Sensors

This section introduces different working mechanisms of bio-interfaced pressure sensors, along with representative materials used for these sensors. For each mechanism, although a diverse set of mechanically active materials can serve as the key components for bio-interfaced pressure sensors, the selection of proper materials requires trade-offs between sensitivity, stability, flexibility, manufacturability, and many other factors. The following subsections separately discuss mechanisms and materials for resistive, capacitive, piezoelectric, triboelectric pressure sensors, and illustrate the pros and cons of different types of mechanically active materials. Additionally, for each mechanism, **Table 1** summarizes the influence of material properties on the performance of bio-interfaced pressure sensors.

© 2023 The Authors. Advanced Materials published by Wiley-VCH GmbH

RIGHTSLINK

15214095, 2024, 43, Downloaded from https://onlinelibrary.wiley.com/doi/10.1002/adma.202205609 by Northwestern University Libraries, Wiley Online Library on [25/10/2024]. See the Terms and Conditions (https://onlinelibrary.wiley.com/terms-and-conditions) on Wiley Online Library for rules of use; OA articles are governed by the applicable Creative Commons License

Table 1. Material-performance relationships for bio-interfaced pressure sensors.

Mechanisms	Parameters	Sensitivity	Linear response range	Response time
Resistive	Gauge factor	+[a)]		
	Elastic range		+	
Capacitive	Modulus of the insulator	–[b)]	+	–
	Dielectric constant of the insulator	+		
Piezoelectric	(Effective) modulus	–	+	–
	Piezoelectric charge constant	+		
	Piezoelectric voltage constant	+		
Triboelectric	Difference in electronegativity	+		

[a)]"+" means positive correlation; [b)]"–" means negative correlation.

2.2.1. Resistive

Resistive-based mechanisms can be adapted to meet many requirements, and the approach typically involves simple classes of materials, basic fabrication schemes, and straightforward measurement electronics.[12,13,20] **Figure 3**A highlights mechanisms and materials for this type of sensor, including devices based on metals (solid and liquid), semiconductors, and conductive composites. Each example involves a change in resistance under external pressures due to a change of: i) dimensions along the direction of external force; ii) dimensions perpendicular to the direction of external force; iii) resistivity; and/or iv) internal structures. The distinct mechanisms and mechanical/electrical properties of these materials leads to sensors with different levels of flexibility/stretchability and sensitivity. Ideal materials properties include large GF, wide elastic range and low sensitivity to temperature and other parameters. Solid metals, when integrated with appropriate structural materials, offer hysteresis-free and fast responses for operation within the elastic range (usually less than 0.3% in material strain).[7,20] Pressure can change the length and/or cross-sectional areas of metal features, resulting in a change in their resistance.[20] Thin films or wires of these materials represent typical embodiments due to their low bending stiffnesses and large initial resistances. These thin films/wires typically mount on cavities[36,63] or cantilevers[64–66] and sometimes integrate into 3D structures[7,12,13,67] or embed in elastomers to amplify deformations under pressure loads.

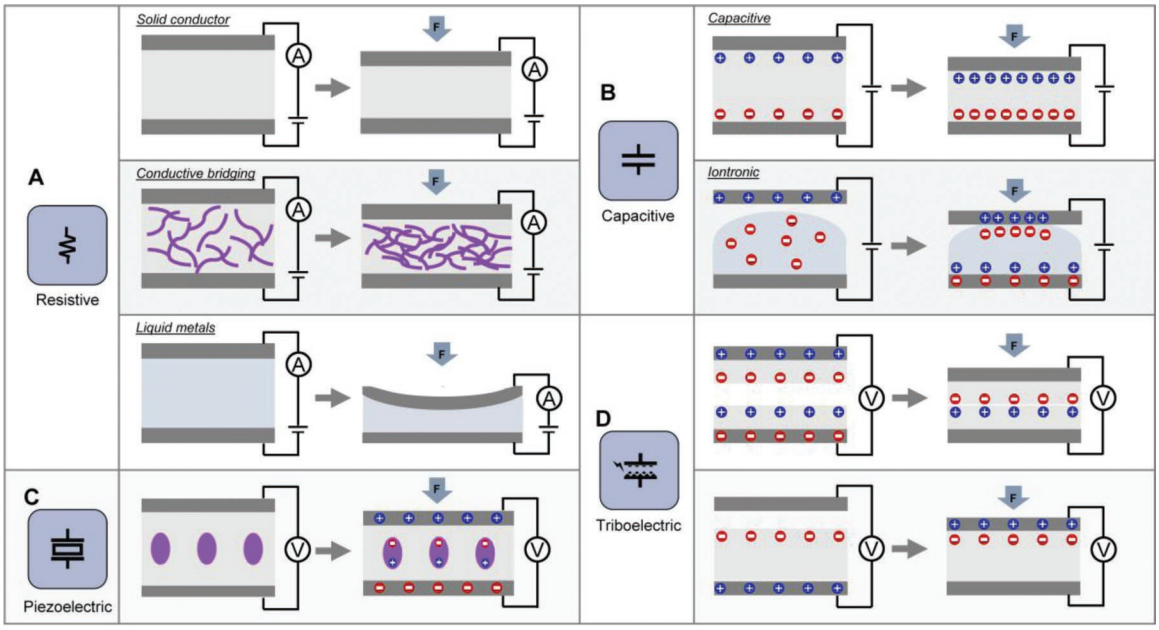

Figure 3. Operational mechanisms for bio-interfaced pressure sensors (deformations not to scale). A) Resistive pressure sensor. Top frame indicates the change of length and area for solid conductors under pressure. Middle frame corresponds to composite materials with conductive bridging effect. Bottom frame illustrates liquid metals that can exhibit large deformations under pressure. B) Capacitive pressure sensor. Top frame illustrates the mechanism of a conventional capacitive sensor with a change in distance under pressure. Bottom frame shows the mechanism of a iontronic sensor based on EDL. C) Piezoelectric pressure sensor. The electric dipoles and amount of surface charges vary with the magnitude of the external pressure. D) Triboelectric pressure sensor. Top frame illustrates a triboelectric sensor based on contact electrification between two polymers. Bottom frame corresponds to a triboelectric sensor based on contact electrification between a polymer and a conductor.

© 2023 The Authors. Advanced Materials published by Wiley-VCH GmbH

RIGHTSLINK

15214095, 2024, 43, Downloaded from https://onlinelibrary.wiley.com/doi/10.1002/adma.202205609 by Northwestern University Libraries, Wiley Online Library on [25/10/2024]. See the Terms and Conditions (https://onlinelibrary.wiley.com/terms-and-conditions) on Wiley Online Library for rules of use; OA articles are governed by the applicable Creative Commons License

Many metals, such as Ti, Pt, Au, Ta, and Ag,[68] exhibit excellent biocompatibility and have Food and Drug Administration (FDA) approvals for chronic use inside the human body. The low resistivity (usually below 0.1 μΩ m) and relatively high sensitivity to temperature (the temperature coefficient of resistance (TCR) is usually in the range of 0.0038–0.005 $°C^{-1}$) of pure metals limit their performance in pressure sensing. By comparison, alloys exhibit higher resistivity (e.g., 1.1–1.5 μΩ m for NiCr) and lower sensitivity to temperature (e.g., TCR is as low as 8×10^{-6} $°C^{-1}$ for CuNi) due primarily to their disordered crystal lattices, which impedes electron transport.[7] The GFs of both pure metals and alloys are ≈2, which is low compared to those of conducting polymers, composites and semiconductors. Considering that the elastic region is usually less than 0.3% in strain, pressure sensors that use metals typically show fractional changes in resistance ($\Delta R/R$) within ±0.6%. Therefore, structural designs and response ranges must be considered carefully based on requirements in biomedical applications (e.g., 80–120 mmHg for BP). One effective approach to improve the GFs of metals relies on motions of micro/nano cracks in thin films.[69,70] For metals with controlled collections of cracks, the conductance of every crack jumps rapidly between zero and a finite value during stretching and releasing. The result is effective GFs that can be as large as 2×10^6.[70]

Liquid metals integrated into channel structures formed in low modulus elastomers enable sensors with soft and flexible characteristics for bio-interfaced applications. Compared with solid metals, liquid metals embedded in these elastomers can respond to dramatic changes in lengths and/or cross-sectional area without plastic deformation, due to the ability of the liquid to flow. Since the resistance is proportional to the resistivity and the length but inversely proportional to the cross-sectional area, these deformations can lead to large changes in resistance (Figure 3A). Eutectic gallium indium (eGaIn) and Galinstan (a gallium-indium-tin ternary alloy, $Ga_{68.5}In_{21.5}Sn_{10}$) are leading candidates for bio-interfaced applications due to their low toxicity.[71–77] Large deformations of conductive traces of these liquid metals generate $\Delta R/R$ up to 2500%,[75] with a strain over 250%.[72] Challenges in these types of sensors are in miniaturization and manufacturability,[78] as the preparation of microchannels and the injection of liquid metals both demand sophisticated approaches in fabrication. Moreover, the formation of surface oxide layers reduces the conductivity of such materials and can cause drift in the performance. The high surface tension (≈624 mN m^{-1}) of these materials can create additional challenges in scalable fabrication.[79,80]

By comparison to metals, the changes in the resistances of semiconductor material structures (e.g., doped Si) result not only from pressure-induced changes in length and cross-sectional area, but also from changes in the resistivity attributed to stress-induced deformation of energy bands (i.e., piezoresistive effect).[20,81,82] The combination of these effects increases the GF to values of more than 100, thereby providing effective means to enhance the sensitivity of pressure sensors from material perspective.[36,56,67,82–84] Representative piezoresistive materials with large GFs, as defined by any material whose resistivity depends on strain, include p-doped monocrystalline Si,[36,56,67,83,84] SiC,[85] semiconductive carbon nanotubes (CNTs),[86] and quasimetallic CNTs.[87] For Si, the doping concentration affects the resistivity, the metal-semiconductor contacts, as well as the GF.[67] Specifically, a boron concentration of $\approx 3 \times 10^{19}$ cm^{-3} in Si leads to a GF of ≈50,[67] while a $\approx 1 \times 10^{19}$ cm^{-3} concentration of phosphorus leads to a negative GF (≈−20.9).[84] A drawback of semiconductors is that integration into flexible, thin films for bio-interfaced pressure sensors can be challenging. The fabrication of most semiconductor devices relies on processes derived from the microelectronics industry, with wafers that have thicknesses from hundreds of micrometers to several millimeters. These thick layers, together with the high modulus of semiconductors (e.g., 140 GPa for Si, 84.8 GPa for GaAs) lead to sensors that have rigid, planar physical characteristics. Advanced manufacturing approaches, such as those based on transfer printing[88,89] and back etching,[90,91] provide means to construct elements of single crystal silicon and other inorganic semiconductors with thicknesses down to 1.4 nm.[92] Since bending stiffness is proportional to the cube of the thickness, these semiconductor structures, sometimes referred to as nanomembranes and often engineered into serpentine[36,93,94] or wavy patterns,[95,96] can provide sufficient flexibility or stretchability for bio-interfaced pressure sensors.

Alternative resistive approaches rely on composite materials in which internal structures or conductive bridges respond to applied pressure (Figure 3A). For sensors that require flexibility and soft mechanical properties, composites usually consist of mixtures of conductive nanoparticles/membranes/plates/tubes within an insulating polymer matrix. In the absence of pressure, these conductive elements form no/few conductive paths through the matrix. With pressure, the distance between these elements decreases to allow quantum tunneling, thereby producing conducting paths. In other cases, these elements form physical contacts that support percolation transport. Both effects lead to changes in resistance with applied pressure.[20,97,98] Typical conductive materials include 0D metals particles (e.g., Pd nanoparticles),[99] 1D conductive nanowires/nanotubes (e.g., CNTs, Ag nanowires, Au nanowires),[100–102] and 2D nanosheets (e.g., reduced graphene oxide, rGO).[103] The insulating matrices range from common papers,[100] to textiles[101,103,104] and polymers.[98,102] Pressure sensors based on these composites offer high GF (e.g., >500,[105] ≈20[106]), but suffer generally from hysteresis and drift, relatively slow response times, and sample-to-sample variations, all as a consequence of the lack of repeatability in forming contacts/tunnel junctions.[20,98]

2.2.2. Capacitive

Compared with resistive sensors, capacitive sensors are less dependent on functional materials. As shown in the top frame of Figure 3B, a capacitive pressure sensor can function properly based on a simple conductor–insulator–conductor structure. External pressures reduce the distance between the conductors to increase the capacitance. Materials for the conductors and insulators, along with the key dimensions, define the capacitances and their sensitivity to pressure. For bio-interfaced sensors, important considerations for the conductors are in their biocompatibility and flexibility. Thin films or nanostructured metals,[40,107] conductive composites,[108,109] hydrogels,[110,111] and liquid metals[112,113] represent some widely explored options.

© 2023 The Authors. Advanced Materials published by Wiley-VCH GmbH

RIGHTSLINK
15214095, 2024, 43, Downloaded from https://onlinelibrary.wiley.com/doi/10.1002/adma.202205609 by Northwestern University Libraries, Wiley Online Library on [25/10/2024]. See the Terms and Conditions (https://onlinelibrary.wiley.com/terms-and-conditions) on Wiley Online Library for rules of use; OA articles are governed by the applicable Creative Commons License

The insulator is essential, as it, along with the structure that defines the layout, determines the sensitivity and initial capacitance. For a given structure under a given pressure, insulators with lower elastic moduli exhibit larger deformations, and therefore higher sensitivity. Typical soft materials for insulators include polymers (e.g., PDMS,[51,114,115] polyamide, polyvinylidene fluoride (PVDF),[116,117] poly(glycerol sebacate)[118]), and polymer composites (e.g., poly(styrene-block-butadiene-styrene) (SBS)/Ag nanoparticles[119] and PDMS/lead zirconate titanate (PZT)[120]). The fillers in these composites have large dielectric constants to improve the initial capacitance. Air can also serve as the insulator, in which case the engineered geometry largely defines the sensitivity. A variety of microstructures[51,54,113,121,122] and mesh patterns[40,119,123–125] can provide effective means for controlling the sensitivity, linear response range, response time, and other features.

Interfacial supercapacitive sensing can further improve the initial capacitance compared with traditional capacitors, with unit-area capacitances of up to 1 μF cm^{-2}[19,126] due to the electric double layer (EDL) that forms at the electrolyte-electrode interface. As shown in the bottom frame of Figure 3B, this type of sensor involves ionic liquids/gels placed between two electrodes. Upon application of pressure, the electrodes deform the ionic liquid/gel, which changes in the interfacial contact area. Such changes in the contact area further influence the EDL capacitances. The key component is the ionic material (i.e., ionic gels and ionic liquids) that generates the EDL through contact with the electrodes. A bias voltage applied to the electrodes induces migration of cations in the ionic liquid to the negative electrode, and anions to the positive electrode, thereby forming the EDL at both electrodes.[127] An example of a sensor based on this mechanism exploits droplets of NaCl in glycerol solution as the ionic liquid, to achieve a sensitivity of 1.58 μF kPa^{-1} and a response time of 260 ms.[126] Advanced versions incorporate arrays of ionic droplets for spatiotemporal mapping of pressure, and others use ionic gels (to replace ionic liquids) for improved mechanical stability.[128] Mixing of different electrolytes with various types of solutions or gels creates many choices for the ionic material. Examples include NaCl in glycerol solution as the ionic liquid, 1-ethyl-3-methylimidazolium tricyanomethanide (EMIM TCM) ionic liquid mixed with PEG diacrylate/2-hydroxy-2-methylpropiophenone (PEGDA/HOMPP) crosslinking hydrogel as the ionic gel,[128] and H_3PO_4 mixed with polyvinyl alcohol (PVA) elastomer matrix as the ionic gel.[129] Structural designs of these or other ionic material layers also influence the sensing performance. For example, electrospinning a fibrous structure of the ionic gel can increase the sensitivity and flexibility,[130] and microstructures (e.g., pyramid)[131–133] of the ionic material layer can improve the sensitivity. A promising use of supercapacitive sensors is in pressure sensing on the human skin, where the skin itself can function as a type of natural ionic material. Such a skin-electrode structure provides a simple and reliable way for measuring pressure compared with traditional supercapacitive sensors.[134] Remaining challenges for iontronic sensors are in improving their response times and in eliminating dependencies on temperature and humidity.[19]

One advantage of capacitive sensors in biomedical applications is that they are suitable for passive wireless operation when incorporated into LRC resonant circuits.[29,135,136] Connecting the capacitive sensor with an inductor and a resistor yields an LRC circuit with a resonant frequency that changes with pressure induced variations in the capacitance. This frequency can be determined wirelessly by coupling to an excitation coil. In this manner, continuous measurements of pressure are possible in internal cavities of the body (e.g., BP and ICP) without percutaneous wires,[136] although with a practical operating range that is usually less than a few centimeters (depending on the dimensions and shapes of the coils[136]).

Limitations with capacitive sensors are in time-dependent parasitic capacitances that can arise from interactions with the human body or other objects in the environment. Advanced circuit approaches (e.g., an on-site integrated circuit can digitize the signal and eliminate the parasitic capacitance in the wires) and packaging schemes can mitigate some of these effects.[137]

2.2.3. Piezoelectric

As shown in Figure 3A,B, both resistive and capacitive sensors demand external power supplies for operation. Piezoelectric materials can generate a potential difference on different surfaces under external force. Measuring the potential difference does not require a voltage bias or current input, thereby establishing the basis for a self-powered type of sensor,[138–140] which reduces the complexity of the sensing system, improves the biocompatibility and flexibility, and extends the lifetime of the sensor. The mechanism relies on a deformation of the solid-state lattice due to applied pressure. For materials with noncentrosymmetric point groups,[141] the geometric centers of cations and anions separate under external forces to generate a polarization (Figure 3C). This polarization induces charge redistribution in conductors placed near the piezoelectric material. The relative permittivity, Young's modulus, electromechanical coupling factor, piezoelectric charge constant (designated as d_{ij}, with a unit of pC N^{-1}), and piezoelectric voltage constant (designated as g_{ij}, with a unit of V m N^{-1}) represent important parameters for piezoelectric materials. The subscripts i and j define the directions of polarization and stress, respectively ($i = 1, 2, 3$; $j = 1, 2, 3, 4, 5, 6$), where 1, 2, and 3 correspond to the direction along *X*, *Y*, and *Z* axis in a Cartesian coordinate system, and 4, 5, and 6 represent shear around the *X*, *Y*, and *Z* axis. For example, d_{31} is the constant that determines the charge generation along the Z direction, for force applied along the *X* direction.

Piezoelectric materials can be classified into crystals,[142] ceramics,[60,143–149] polymers,[14,150–153] and heterogeneous combinations of them.[144,147] Natural crystals, such as quartz and $LiNbO_3$, have high mechanical quality factors and electromechanical coupling coefficients,[142] and are most commonly used for applications that require mechanical actuation. Ceramics have high piezoelectric charge constants, but their brittle nature can lead to breakage and cracking in bio-interfaced applications.[154,155] Widely used piezoelectric materials include PZT,[145,149] zinc oxide (ZnO),[146–148] barium titanate ($BaTiO_3$),[60,144] aluminum nitride (AlN),[143,155] and lead magnesium niobate–lead titanate (PMN-PT).[156] PMN-PT has the highest piezoelectric charge constant (2000–3000 pC N^{-1}).[157] Values for other ceramics range from dozens to hundreds of

© 2023 The Authors. Advanced Materials published by Wiley-VCH GmbH

RIGHTSLINK
15214095, 2024, 43, Downloaded from https://onlinelibrary.wiley.com/doi/10.1002/adma.202205609 by Northwestern University Libraries, Wiley Online Library on [25/10/2024]. See the Terms and Conditions (https://onlinelibrary.wiley.com/terms-and-conditions) on Wiley Online Library for rules of use; OA articles are governed by the applicable Creative Commons License

pC/N. Although PZT can be used in nanomembrane form for bio-interfaced sensors,[158,159] its high modulus (e.g., 63 GPa for PZT) and toxicity (e.g., Pb in PZT and PMN-PT) represent disadvantages.

On the contrary, piezoelectric polymers have comparatively smaller piezoelectric coefficients,[144,155] but their low modulus and excellent biocompatibility[160] are attractive for applications as bio-interfaced pressure sensors. β-phase polyvinylidene fluoride (PVDF)[14,150,151] and poly(vinylidene fluoride-*co*-trifluoroethylene) P(VDF-TrFE)[152,153,161] represent two common piezoelectric polymers with large piezoelectric coefficients (PVDF: d_{31} = ≈23 pC N^{-1} d_{33} = ≈–33 pC N^{-1} g_{31} = ≈220 mV m N^{-1} g_{33} = ≈–330 mV m N^{-1}; P(VDF-TrFE): d_{31} = ≈10.7 pC N^{-1} d_{33} = ≈–33.5 pC N^{-1}). The piezoelectricity in these cases originates from the asymmetric distribution of H (positive charge) and F (negative charge) atoms in the β-phase. Constructing them as nanowires or nanofibers enables high sensitivity (up to 0.1 Pa[152]), and large mechanical deformations (up to 6.2% in tensile strain, 5 times larger than that of thin films[162]) without fracture.[146,151,152] Devices that exploit these features include sensors for the noninvasive measurement of pulsatile blood flow, where the changes in pressure can be small (≈1.05 kPa[163]), and of plantar pressure where the body weight (70 kg for adult male) can cause severe deformations.

Mixing different types of piezoelectric materials provides a means to balance the piezoelectric and mechanical properties. For example, dispersing piezoelectric ceramics in piezoelectric polymers yields materials with low modulus and high piezoelectric charge constants. Examples of the use of such materials include sensors that incorporate ZnO nanoneedle/PVDF films[147] and $BaTiO_3$ in a PVDF matrix.[144] The mixtures can also exploit passive polymers (i.e., polymers without piezoelectricity) as matrices for dispersing piezoelectric particles. Such piezoelectric-passive polymer composites have categories including 0-3, 1-3, ..., 2-2, 3-3 depending on the connectivity of the active phase (piezoelectric materials) and the connectivity of inactive phase (passive polymers).[164] The first digit represents the number of connectivity of piezoelectric materials, and the second digit refers to this value for passive elastomers (e.g., a phase self-connected in all *x*, *y*, and *z* directions corresponds to type "3"; a phase self-connected only in the *z* direction corresponds to type "1"). Examples are in a 0-3 type PZT/PDMS composite,[165,166] a 1-3 type PMNT/epoxy composite,[167] and a 2-2 type PZT/epoxy composite.[168] The connectivity status decides the electrical and mechanical properties of the composites. For example, for a 3-3 type composite, the connections of passive polymers in all three directions provide sufficient mechanical strength, and the connection of piezoelectric materials in all three directions allows for continuous electrical connections and large charge constants. Though the passive polymers do not enhance the piezoelectric constants, the range of options is broad, and includes soft elastomers (e.g., PDMS[165,166]), biodegradable materials (e.g., s,[169] PLA[170]), and many others.[167,168,171]

The most significant drawback of piezoelectric sensors is in their limited ability to quantify static pressure values. The measured voltage from piezoelectric sensors is typically an impulse signal that exists only in the transition of different pressures, due to the large internal impedance of the devices.[172] As a result, in biomedical applications, piezoelectric sensors are most suitable for measuring fluctuating pressures, such as those associated with arterial blood flow[147] or with physical motions at organ surfaces.[144,154]

2.2.4. Triboelectric

As with piezoelectric pressure sensors, triboelectric devices convert changes in pressure into electrical outputs in a self-powered mode.[10,61,62] The differences in electronegativity, surface texture, and other subtle features, between two materials in contact produce charge separations due to contact electrification.[61,62,173–176] This phenomenon occurs with almost all types of materials, including semiconductors (e.g., Si, Si_3N_4, PEDOT:PSS),[177] metals (e.g., Al, Cu, Ni),[62,178,179] polymers (e.g., PTFE, PDMS, Kapton, PET, polyamide),[61,62,173,174] and liquids (e.g., pure water, oil).[180,181] The top and bottom frames of Figure 3D illustrate contact electrification between two polymers and between a polymer and a conductor, respectively. In the former case, net charges appear at the surfaces of the polymers. Pressure changes the gap distance and causes charge redistribution on the conductors due to electrostatic induction. Similar mechanisms apply to the latter case. Here, the conductor serves as a layer for both electrification and electrostatic induction. With such configurations, the total amount of charges on the two conductors is not zero.

Although triboelectric pressure sensors can be built from a variety of materials, applications in biomedicine require flexibility, stretchability, biocompatibility, and high surface charge density upon contact electrification. Based on the triboelectric series,[176,182] PTFE and PDMS possess high electronegativity (surface charge density: ≈–113.06 μC m^{-2} for PTFE and ≈–102.05 μC m^{-2} for PDMS when contacting with mercury),[176] whereas certain rubbers possess low electronegativity (surface charge density: ≈2.49 μC m^{-2} for Oil-Resistant Buna-N Rubber and ≈2.95 μC m^{-2} for Food-Grade Oil-Resistant Buna-N/Vinyl Rubber when contacting mercury).[183] Thin films of these materials are biocompatible and flexible/stretchable, and are thus promising candidates for the applications considered here. These materials can also be engineered with micro/nanostructures through soft lithography,[61,62,174] plasma treatment,[10] laser ablation,[184,185] and other approaches.[186] The micro/nanostructures substantially increase the surface areas of the materials, thereby improving the effective surface charge densities. The amplitude of the output signal (i.e., the sensitivity) of a triboelectric device built with micro/nanostructured materials can be enhanced by a factor of six, compared with the case without micro/nanostructures.[61]

The surface charge density influences the sensitivity of triboelectric pressure sensors. Charges generated by contact electrification depend not only on the electronegativity of the materials, but also on the temperature, humidity, surface texture, and others.[187–189] Accurate operation of the sensors, therefore, may require rigorous encapsulation and/or frequent calibration. Most triboelectric pressure sensors reported in the literature are suitable for detecting changes in pressure due to their high sensitivity (up to 51 mV Pa^{-1}),[190,191] but are less able to provide quantitative values of the pressure.

© 2023 The Authors. Advanced Materials published by Wiley-VCH GmbH

RIGHTSLINK

15214095, 2024, 43, Downloaded from https://onlinelibrary.wiley.com/doi/10.1002/adma.202205609 by Northwestern University Libraries, Wiley Online Library on [25/10/2024]. See the Terms and Conditions (https://onlinelibrary.wiley.com/terms-and-conditions) on Wiley Online Library for rules of use; OA articles are governed by the applicable Creative Commons License

15214095, 2024, 43, Downloaded from https://onlinelibrary.wiley.com/doi/10.1002/adma.202205609 by Northwestern University Libraries, Wiley Online Library on [25/10/2024]. See the Terms and Conditions (https://onlinelibrary.wiley.com/terms-and-conditions) on Wiley Online Library for rules of use; OA articles are governed by the applicable Creative Commons License

Table 2. Structure–performance relationships for bio-interfaced pressure sensors.

Structures	Parameters	Sensitivity	Linear response range	Response time
3D geometry	Modulus of the encapsulation	–	+	–
Micropatterns	Dimension of the micropatterns	–		
	Spacing of the micropatterns			+
Mesh and fiber	Density of the fiber	+		
Cavity structures	Lateral dimensions of the cavity	+		
	Thickness of the top membrane	–	+	
	Modulus of the top membrane	–	+	–

2.2.5. Other Mechanisms

Other bio-interfaced pressure sensors exploit permanent magnets, optical elements, or combinations of the mechanisms mentioned in the preceding sections, to achieve interesting properties. Magnetic pressure sensors usually consist of a magnetic field detector, and a layer of hard magnetic material to generate a magnetic field. Pressure and other mechanical stimuli deform the magnetic material and cause redistributions of the magnetic field.[192–196] A changing flux density associated with dynamic pressure can be captured through an inductive coil in a self-powered manner. For static pressure, a Hall sensor or giant/tunneling magnetoresistance sensor can serve as the magnetic field detector. Bio-interfaced pressure sensors require flexible/stretchable magnetic films. A mixture of magnetic particles (e.g., NdFeB) in polymer matrices represent the most promising candidate for this purpose.

Optical sensors leverage various types of photonic elements to enhance the performance and expand the modes of operation.[2,197,198] Changes in wavelengths, polarization states, or other properties of light resulting from alterations in a propagation medium can reflect the amplitudes and/or positions of sources of applied pressure. A representative example incorporates a dual-core (i.e., clear core and dyed core) optical fiber design,[197] where the chromaticity and intensity of the output light can determine the location, magnitude, and modes of deformation of the fiber.

Combining different mechanisms together provides an additional approach to improve the performance of bio-interfaced pressure sensors. Examples include a pressure sensor based on both piezoresistive and piezoelectric effects to allow for measurements of static and dynamic pressure;[199,200] a pressure sensor based on a porous nanocomposite (i.e., mixture of CNT and silicone) with both piezoresistive and piezocapacitive properties to offer high sensitivity over a wide pressure range (3.13 kPa^{-1} within 0–1 kPa, 0.43 kPa^{-1} within 30–50 kPa);[201] and a biomimetic robot skin that incorporates electrical impedance tomography and acoustic tomography to measure both static and dynamic stimuli.[202]

2.3. Engineered Material Structures

Though intrinsic properties of materials are important, as outlined in previous sections, certain structural designs can compensate for nonideal material characteristics and they can greatly enhance the performance. Common designs include 3D geometries, micropatterns, mesh and fiber layouts, and cavity structures. For each design, the structural parameters can affect the performance of bio-interfaced pressure sensors, as summarized in **Table 2**.

2.3.1. 3D Geometry

All mechanisms for sensing pressure require deformation of materials, the magnitude of which correlates with that of an output signal. 3D structures can be designed to enhance these deformations (>≈100 μm) in the direction perpendicular to the substrate, compared to that possible with planar devices (less than the thickness of the material, usually <1 μm), thereby providing benefits in pressure sensing. Various manufacturing procedures, such as stress-induced-bending[203,204] and compressive buckling[7,12,13,67,205] can yield 3D structures and devices in a parallel fashion. A promising approach exploits conventional strain gauges bent or buckled into a 3D form to detect forces in the vertical direction (i.e., normal pressure). An example uses a thin chromium layer (100 nm, internal tensile stress of ≈2 GPa[206]) on the top to bend layers of silicon nitride (SiN, 200 nm) and Si (2.5 μm) on silicon-on-insulator (SOI) wafer into curved beams.[207] The p-doped silicon piezoresistive element between the silicon nitride and silicon nanomembrane serves as a 3D strain sensor (i.e., pressure sensor). Combining four such sensors in different lateral directions allows for simultaneous detection of normal pressures and shear forces.

A recently developed compressive buckling approach can transform 2D patterns into 3D structures with diverse geometries, including curved filaments,[205] origami constructs,[208] multilayer meshes,[209] and many others.[210,211] Origami structures can be formed by controlling the thicknesses of 2D precursors to concentrate strains at small areas, thereby allowing for optimal positioning of strain sensors.[212] Devices that utilize such 3D buckled structures include those based on resistive,[7,12,13,67] capacitive,[213] and piezoelectric effects.[14] **Figure 4**A presents a 3D pressure sensor for bio-interfaced applications.[12] The structure consists of three layers, where a gold strain gauge (thickness: 100 nm) lies between two layers of polyimide (PI, thickness of the top layer: 4 μm, thickness of the bottom layer: 6 μm). A soft elastomer encapsulates the structure to provide an elastic restoring force and to enhance the robustness. Adjusting the modulus of the elastomer offers a means to tune the sensitivity

© 2023 The Authors. Advanced Materials published by Wiley-VCH GmbH
RIGHTSLINK

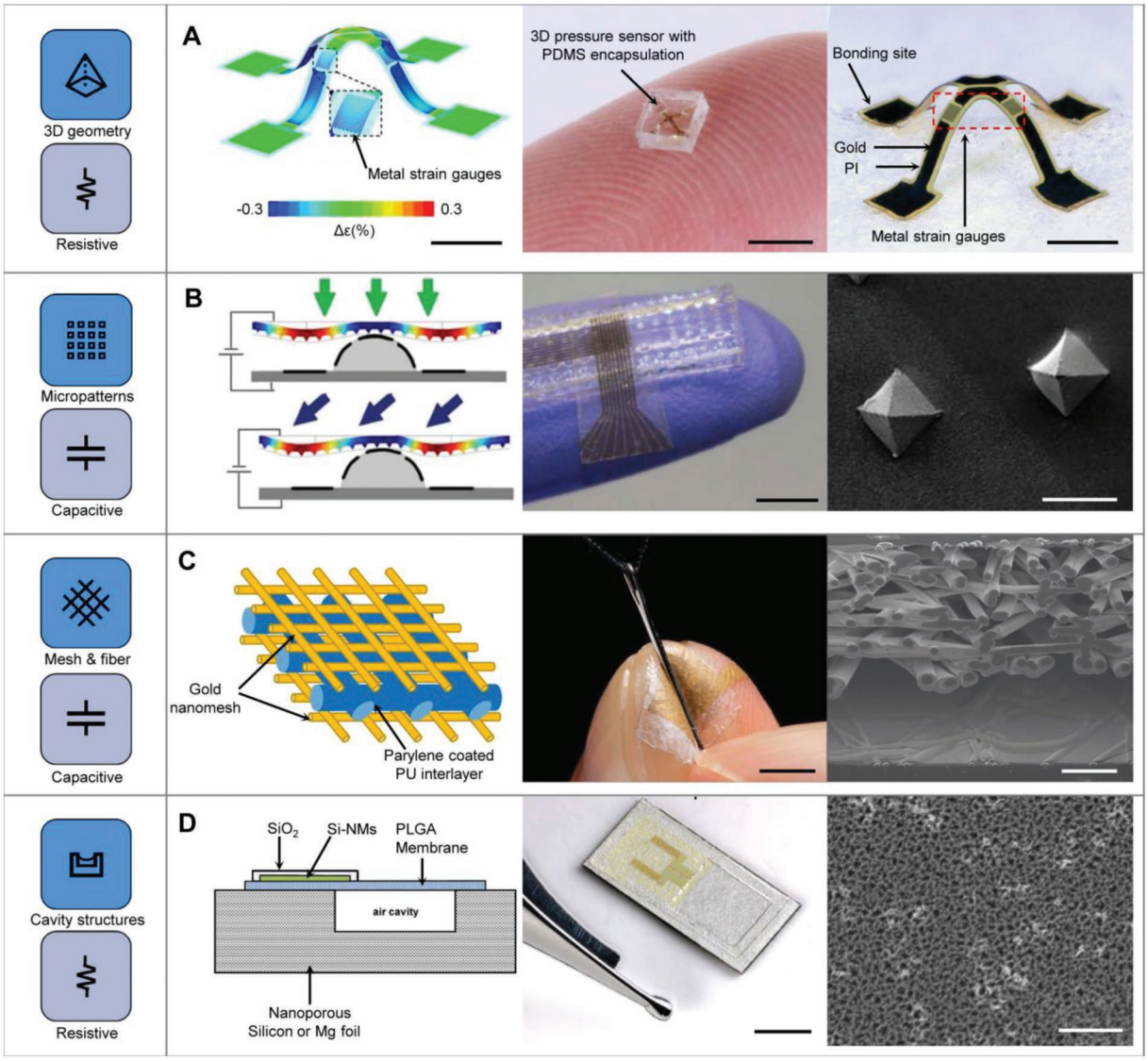

Figure 4. Engineered structures for bio-interfaced pressure sensors. A) Simulated distribution of strains under normal pressure of 200 kPa (left), optical image of a 3D pressure sensor embedded in a soft elastomer (middle), and magnified optical image of a 3D pressure sensor (right). Scale bars, 500, 4, 500 µm, from left to right. Reproduced with permission.[12] Copyright 2020, American Association for the Advancement of Science. (B) Schematic illustration of the deformations of the device under mechanical stimuli (left), optical image of the pressure sensor with micropattern (middle), and SEM image of the micropattern (right). Scale bars, 5 mm for the middle frame and 30 µm for the right frame. Reproduced with permission.[121] Copyright 2018, American Association for the Advancement of Science. C) Schematic illustration of the Au-PU-Au sandwich structure (left), optical image (middle), and cross-sectional SEM image (right) of a nanomesh pressure sensor. Scale bars, 5 mm for the middle frame and 5 µm for the right frame. Reproduced with permission.[40] Copyright 2020, American Association for the Advancement of Science. D) Cross-sectional illustration of the cavity structure (left), optical image of a cavity-based pressure sensor (middle), and SEM image of the porous substrate (right). Scale bar, 2 mm for the middle frame and 150 nm for the right frame. Reproduced with permission.[36] Copyright 2016, Springer Nature.

and customize the sensing range to match needs for different scenarios, such as the evaluation of pressure inside compressive stockings[13] which require sensitivity up to 1.5 $\times 10^{-4}$ kPa^{-1}, and the continuous monitoring of pressure at skin-prosthetic interfaces which demand response range as high as 350 kPa.[12] Here, PDMS serves as the encapsulation layer, since its modulus can be adjusted easily (e.g., by changing the crosslinking density via control over the ratio of base and curing agent, or the curing temperature) to meet different requirements.

Other opportunities for pressure sensors based on 3D geometries include large-scale, high-density spatiotemporal mapping,[7,67] enabled by the scalability and parallel nature of the manufacturing approach. Challenges for this type of sensor are in design and optimization strategies that capture the nonlinear mechanics associated with the 2D to 3D geometry transformation process, across dimensions that range from the millimeter (lateral dimension or height of the structure) to the nanometer (thickness of metal or doped-Si in the strain gauges) scale.

© 2023 The Authors. Advanced Materials published by Wiley-VCH GmbH

RIGHTSLINK

15214095, 2024, 43, Downloaded from https://onlinelibrary.wiley.com/doi/10.1002/adma.202205609 by Northwestern University Libraries, Wiley Online Library on [25/10/2024]. See the Terms and Conditions (https://onlinelibrary.wiley.com/terms-and-conditions) on Wiley Online Library for rules of use; OA articles are governed by the applicable Creative Commons License

15214095, 2024, 43, Downloaded from https://onlinelibrary.wiley.com/doi/10.1002/adma.202205609 by Northwestern University Libraries, Wiley Online Library on [25/10/2024]. See the Terms and Conditions (https://onlinelibrary.wiley.com/terms-and-conditions) on Wiley Online Library for rules of use; OA articles are governed by the applicable Creative Commons License

2.3.2. Micropatterns

Micropatterns refer to microscale structures incorporated into the sensitive elements of the sensor to control and enhance the response characteristics. Surface relief in the form of arrays of hemispheres,[174,214,215] micropyramids,[51,113,121,131,216,217] micropillars,[132] microcones,[133] and nonuniform bumps[129,218] offer means to tailor the sensitivity and range of operation to meet requirements.[51,219] Additionally, such structures can minimize effects of hysteresis and drift that can occur in viscoelastic materials for mainly two reasons. First, the presence of air in the gaps between the microstructure features allows the materials to bend downward, to reduce the material strains compared to those that would otherwise follow from compression.[51] Second, the microstructure can effectively reduce mechanical losses caused by adhesion between different layers.[220] Micro/nanopores introduced into elastomeric materials such as PDMS can reduce their effective modulus (from 2.61 to 182 kPa for 10:1 PDMS[115]) and enhance their sensitivity.[102,115,221] Microchannels, often used together with liquid metals, can be designed to enhance local deformations to create conductive features that define resistances and enable incorporation into Wheatstone bridge structures for readout.[222]

This strategy of structural engineering is applicable across resistive,[214,215,221,223–229] capacitive,[51,54,113,121,122] iontronic,[131–133] piezoelectric,[161,230] and triboelectric[61,174] pressure sensors, with materials ranging from silicone elastomers,[51,54,61,122,230] and polymer composites,[223,225–227] to ionic gels.[131,133] Figure 4B shows a representative example of a pressure sensor that incorporates hemispherical structures (or "hills" as described in the literature). Inspired by the spinosum of human skin, the sensor consists of a bottom layer with a hemisphere array, a middle polyhydroxybutyrate/polyhydroxyvalerate (PHB/PHV) dielectric layer, and a top layer with a micropyramid array. Notably, the dielectric layer must be thin to realize a high initial capacitance. The mechanical robustness of thin layers of PHB/PHV make this material a promising candidate for such capacitive pressure sensors. Upon application of pressure, the contact area increases and the separation distance between the electrodes decreases, leading to an increase in capacitance. The bottom layer incorporates a molded hemisphere structure array, where an individual hemisphere covers 25 capacitors (90 000 μm^2). This structure can be used to distinguish normal force and shear force.[121] The dimensions and distributions of the micropyramid array can influence the sensor performance. In the example shown in Figure 4B, smaller micropyramids contribute to higher sensitivity, whereas shorter separation distances between micropyramids lead to faster response times.

Remaining challenges with pressure sensors based on micropatterns include structural stiffening that limits the performance in the high-pressure regime. Most elastomers utilized in such pressure sensors have Poisson's ratios close to 0.5 and are nearly incompressible, which causes stiffening at large strains where the Gaussian elasticity of polymer chains does not apply.[19,231] Other disadvantages are in low sensitivity above certain pressure levels due to a saturation of the contact area,[121,221] and long response/recovery times in the low-pressure range for porous designs.[221]

2.3.3. Mesh and Fiber

Mesh and fiber structures are of interest for creating soft, flexible, air permeable, and durable features.[146,151,152] Techniques for fabrication include electrospinning,[40,123–125,232] thermal drawing,[233] and 3D printing[234–236] for sensors that exploit resistive ,[100,101,103,232,237] capacitive,[40,119,123–125,238] piezoelectric[233] and triboelectric[10] mechanisms, with materials ranging from metal nanomesh constructs and conductive fibers as electrodes,[40,232,239] nanofibers of polymers (e.g., PVDF-HFP, PVDF, and PLGA-PCL) as dielectric layers,[123–125,130] fibers coated with conductive materials (e.g., graphene oxide-coated silk fabrics, textile-structured CNT-coated cotton fabrics) as resistive materials,[101,103] piezoelectric composite (e.g., P(VDF-TrFE)/$BaTiO_3$) fibers as piezoelectric materials,[233] and woven PTFE and silver coated nylon yarn as materials for contact electrification.[10,240] In all cases, pressure generates a change in resistance, capacitance or voltage.

Functional materials in mesh and fiber structures can be engineered into textiles for wearable physiological monitoring.[40,101,103] Ultrathin, porous, and open-mesh layouts also allow sensors to be attached to the skin in a comfortable or even imperceptible manner.[40,130] A representative example in Figure 4C highlights a pressure sensor that involves mesh patterns in nanoscale geometries[40] for monitoring finger manipulation. The sensor incorporates a nanomesh bottom electrode in gold, a parylene-coated (thickness: 200 nm) polyurethane (PU, thickness: 10.5 μm) nanomesh interlayer with an air gap (distance: 1 μm), a gold nanomesh top electrode, and a PU nanomesh-embedded passivation layer (thickness: 2.5 μm). Here, electrospinning of PVA nanofibers forms a sacrificial supporting layer. Thermal vacuum deposition of Au (thickness: 100 nm) on the PVA, followed by dissolving the PVA in water, yields the nanomesh pressure sensor. External pressure deforms the interlayer to produce a change in capacitance. Major factors that influence the sensitivity include the density of PVA nanofibers for top Au nanomesh electrode, and the stiffness of materials for the interlayer. Specifically, denser PVA nanofibers lead to higher sensitivity. PU coated with a layer of parylene can provide optimal stiffness to enhance the sensitivity. The sensitivities are 0.141 kPa^{-1} for pressures less than 1 kPa and 0.010 kPa^{-1} for pressures between 1 to 10 kPa. The ultrathin nature of this nanomesh sensor (total thickness: ≈14 μm) is of interest because it does not interfere with natural human tactile sensation. These same features of pressure sensors that utilize mesh or fiber structures make them well suited for other bio-interfaced applications, with excellent levels of stretchability, water resistance, and breathability.[40,232,241]

2.3.4. Cavity Structures

The structures introduced in the previous sections (Sections 2.3.1–2.3.3) are most well suited for measuring contact pressure between solid materials, especially at soft tissue interfaces. Measurements of pressures from gases or liquids are best performed using sealed cavity structures. Deformations of a thin membrane that seals the cavity directly reflect the outside

© 2023 The Authors. Advanced Materials published by Wiley-VCH GmbH

fluid pressure, with demonstrated applications in monitoring of BP, ICP, and bladder pressure.

Pressure sensors of this type include two key elements: a relatively rigid structure as the base of the cavity and a flexible membrane on top. Deformations of the membrane cause a change in either the capacitance (when the top membrane and bottom cavity forms a capacitor[242]) or the resistance (when resistive materials are integrated in the membrane[36]). Parameters that define the performance include the lateral dimensions and depth of the cavity, the modulus and thickness of the membrane, the properties of the materials that fill the cavity, and the nature of the seal that defines the cavity. Specifically, increasing the lateral dimensions or reducing the flexural rigidity of the membrane increases the sensitivity. Increasing the depth of the cavity expands the range of allowed deformations of the membrane, thus increasing the response range. Sealed cavities allow for measurements of both fluid and contact pressures when encapsulated with soft elastomers (e.g., TakkTile sensors based on MEMS barometers[243,244]). Open cavities are suitable only for contact pressure.

Capacitive sensors incorporate electrodes located at the top membrane and the bottom of the cavity. An example of a device of this type includes a PLGA cavity with a Zn electrode on the membrane and a Mg electrode on the bottom trench, as the basis for a bioresorbable pressure sensor for ICP.[245] In another case, a fixed plate of Si_3N_4 and a moving plate in poly-Si form a MEMS capacitive sensor for monitoring motions of the skin near the wrist due to pulsatile flow of blood through near surface arteries.[246] Unconventional cavity designs can improve the performance and form factor. For instance, a single-sided ionic material and human skin can serve as electrodes of a capacitor for pressure sensing. Here, the cavity exploits two supporting elements that separate the ionic electrode from the skin electrode, thereby yielding a thin device naturally integrated with the skin.[242]

Resistive pressure sensors that exploit the cavity design rely on sensitive materials integrated as part of the membrane, such as doped silicon,[36,83] silicon carbide[247] and metals.[63] The cavity under the membrane provides a large space for deformation upon exposure to external pressure, with a sensitivity that can be much larger than that possible in sensors without a cavity.[83] Figure 4D presents a bioresorbable sensor that consists of a membrane of PLGA (thickness: 30 μm) that supports a patterned resistive trace of P-type doped Si (thickness: ≈200 nm; GF: ≈30) as the top seal of a cavity defined in nanoporous Si (dimension: 0.67 mm by 0.8 mm by 0.03 mm).[36] An encapsulation layer of SiO_2 (thickness: ≈100 nm; deposited through electron-beam evaporation) protects the doped silicon from biofluids. The nanoporous feature substantially increases the area, thereby accelerating dissolution in vivo. The sensor can monitor pressure in various body cavities, including the brain, the intra-abdominal space, and compartments of the leg. High sensitivity requires cavities with large lateral dimensions or with very thin membranes. For example, for a Si membrane with a thickness of 3–6 μm, a sensitivity of 0.0117 kPa^{-1} corresponds to a cavity of ≈1 by 1 mm.[248] The trade-off between overall dimension/spatial density/flexibility and accuracy/sensitivity demand careful optimization to address the needs of specific applications.

3. Devices and Systems

As discussed previously, pressure sensors with soft and thin form factors enable placements on delicate tissues for noninvasive measurements over long periods of time. This section presents various technologies of this sort, with an emphasis on those that enable measurements in or on the skin, heart, and brain. Pressures inside or at the interfaces with these organs provide important information on the evaluation of skin conditions, surgical procedures, cardiovascular diseases, and many other factors related to human health.

3.1. Skin-Interfaced Pressure Sensors

Skin-interfaced sensors can provide information on externally applied pressures (e.g., pressure between skin and other objects),[249–252] and they can also be used to approximate pressures inside the body. Advanced sensors have thin, soft form factors with the ability to be arranged into multiplexed arrays or distributed components, with capabilities in wireless data communication.

3.1.1. Pressure Sensing at a Single Point

In many scenarios, monitoring of pressure at a single location can provide sufficient information. Examples in biomedicine involve the measurement of contact pressures at specific locations to prevent skin ulcers or peripheral nerve injuries,[253] the evaluation of pressure during compression therapy,[13] and the estimation of BP through a noninvasive pressure sensor near the artery. In particular, tracking of changes in BP can be accomplished with a sensor positioned above the radial artery.[9,254,255] **Figure 5**A presents a wired sensor for this purpose with a three-layer architecture, which includes a nanofibrous ionic interlayer (thickness: ≈50 μm, formed by electrospinning) with patterned conductive fabrics above and below (thickness: ≈300 μm). The ionic material is a gel-based matrix of P(VDF-HFP) with 1-Ethyl-3-methylimidazolium bis(trifluoromethylsulfonyl)imide (EMIM TFSI, weight ratio 1:1). These flexible thin films allow the sensors to form conformal contact directly with the human hand or indirectly through a glove. The device offers a high sensitivity of 114 nF kPa^{-1} and a pressure resolution of 2.4 Pa. Although many bio-interfaced pressure sensors exploit wired connections for proof-of-concept demonstrations,[9,100,222,227,256] wireless operation eliminates restrictions in motion that follow from these physical tethers. Techniques for wireless communication range from passive approaches based on LRC circuits, to standard wireless protocols based on near-field communications (NFC) and Bluetooth low-energy (BLE) systems.

As explained previously, an LRC resonance circuit employs a capacitive pressure sensor and an inductor for wireless sensing. Deformation in a pressure sensor leads to a change in capacitance that shifts the resonance frequency ($f = \frac{1}{2\pi\sqrt{LC}}$). An external readout coil can detect the resonance frequency wirelessly through inductive coupling. Demonstrations of this method include wireless monitoring of pressures on the wrist,

© 2023 The Authors. Advanced Materials published by Wiley-VCH GmbH

RIGHTSLINK

15214095, 2024, 43, Downloaded from https://onlinelibrary.wiley.com/doi/10.1002/adma.202205609 by Northwestern University Libraries, Wiley Online Library on [25/10/2024]. See the Terms and Conditions (https://onlinelibrary.wiley.com/terms-and-conditions) on Wiley Online Library for rules of use; OA articles are governed by the applicable Creative Commons License

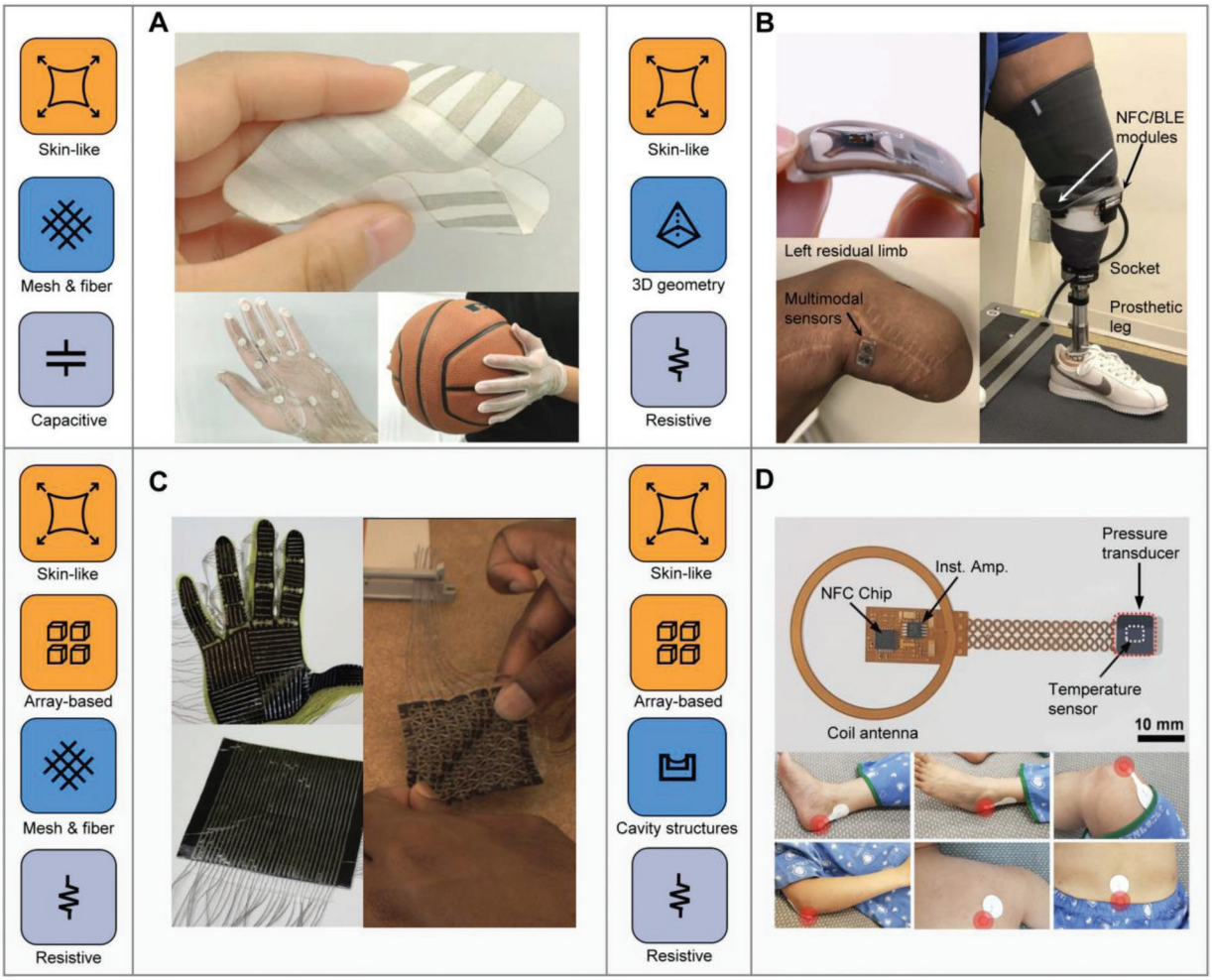

Figure 5. Noninvasive bio-interfaced pressure sensors. A) Wearable ionic pressure sensor that incorporates mesh structures. Reproduced with permission.[130] Copyright 2017, Wiley-VCH. B) Wireless, battery-free pressure sensor for prosthetic users. Reproduced with permission.[12] Copyright 2020, American Association for the Advancement of Science. C) Pressure sensor array for spatiotemporal mapping. Reproduced with permission.[260] Copyright 2019, Springer Nature. D) Wireless, distributed array of sensors for pressure mapping across the entire body. Reproduced with permission.[63] Copyright 2021, Springer Nature.

on a shoe insole, and in a pulmonary artery, around a facial artery, and inside a cranial cavity.[29,135,136,245,257,258] The scheme applies only to capacitive sensors and the readout electronics (coil and impedance analyzer) can be large and bulky.

On the other hand, NFC offers an alternative battery-free communication scheme that avoids these disadvantages. The NFC interface can support both data and energy transmission. Figure 5B shows a thin device of this type that consists of a 3D pressure sensor and an NFC circuit on a flexible printed circuit board (FPCB). The device design allows insertion into a prosthetic socket for continuous monitoring of the pressure at the interface with the skin of a residual limb. The soft silicone elastomer and the thin films of polyimide and metals render skin-like features for the pressure sensor, thereby supporting comfort for use in prosthetic sockets. Here, digitized pressure information passes wirelessly to a battery-powered circuit module (including an NFC coil and an NFC reader) mounted outside the prosthesis that also supports BLE transmission to a portable electronic device for data recording and analysis.[12]

3.1.2. Pressure Mapping

Multiple sensors arranged in array formats create additional opportunities in pressure measurements. Imitating human grasp for accurate robotic control[7,121,130,175,222,239,259,260] and spatiotemporal mapping of body pressure over a large area[56,63] represent two important applications. Figure 5C shows an array of 548 resistive sensing elements, where each node consists of an overlap of an orthogonal thread network (3-ply stainless steel conductive threads, 12 μm in fiber diameter, 0.34 mm in overall diameter) and a force-sensitive thin film (3 M Velostat electrically conductive copolymer, thickness: 0.1 mm) sandwiched between.[260] The array can be integrated on a glove for quantifying pressure distributions during grasping of different objects. A deep learning framework can analyze the results for object identification. In this example, an analog multiplexer scans through each row to record the corresponding resistances at each sensing point. Additional amplifiers and switches ground the sensing elements in a programmed sequence

© 2023 The Authors. Advanced Materials published by Wiley-VCH GmbH

RIGHTSLINK

15214095, 2024, 43, Downloaded from https://onlinelibrary.wiley.com/doi/10.1002/adma.202205609 by Northwestern University Libraries, Wiley Online Library on [25/10/2024]. See the Terms and Conditions (https://onlinelibrary.wiley.com/terms-and-conditions) on Wiley Online Library for rules of use; OA articles are governed by the applicable Creative Commons License

to eliminate crosstalk.[258,261] Another option for spatiotemporal mapping without crosstalk involves transistors at each sensing element. Flexible transistors for this purpose can use Si nanomembranes,[262] organic semiconductors[263] or various other thin-film materials,[264,265] with straightforward paths for integration with circuits, multiplexing capabilities, and on-site amplification.

In some applications, pressure mapping does not require high spatial density, but must cover large areas (e.g., across the whole body).[56,63] In such cases, the sensors can be sparsely arranged into distributed arrays. Figure 5D demonstrates this type of multisite pressure sensing system,[63] where eight pressure sensors distribute across different locations of the body (heel, malleolus, knee, elbow, scapulae, and sacrum). A metal strain gauge (made of Cr/Au bilayer, thickness: 10 nm/30 nm) sandwiched between PI films (thickness of the upper film: 75 μm; thickness of the lower film: 10 μm) adheres on top of a trench (lateral dimension: 2 mm × 2 mm; depth: 0.15 mm), and operates as the resistive sensing element. Here, each sensing element incorporates an NFC wireless module to pass pressure values to a reader device in a wireless manner.

3.2. Invasive Pressure Sensors

Besides pressures at the skin interface, many cavities inside body experience pressures that are related to health status. Minimally invasive, miniaturized and biodegradable pressure sensors minimize risks to the patient, because the former reduces the dimensions of the incisions needed for implantation, and the latter eliminates requirements for surgical extraction.

3.2.1. Minimally Invasive Sensors

Such devices enable evaluations of pressures inside body cavities, such as IOP,[3,4] ICP[135] and BP,[8,11] through small incisions. Materials used for biocompatible encapsulation of these sensors include parylene-C,[3,11] silicone elastomers,[3,4,7,266] PI,[4,8,135] polycaprolactone,[267] and silicon dioxide.[268] An example is in an FDA-approved device (CardioMEMS) that consists of a capacitive pressure sensor and an inductor encapsulated in a quartz housing. The device has a dimension of 15 mm by 3.4 mm by 2 mm, to allow implantation into the pulmonary artery through a 12 Fr introducer sheath in a minimally invasive manner. The device monitors pulmonary hypertension to aid in management for heart failure.[258,269]

An alternative type of miniaturized sensor measures the pressure at the interfaces between surgical tools or implantable devices and biological surroundings for diagnostic and therapeutic procedures. Examples integrate pressure sensors on catheters,[7,270,271] endoscopes,[272,273] or stents.[274,275] The flexibility and stretchability of soft pressure sensors of this type create opportunities for spatiotemporal mapping. **Figure 6**A shows a resistive pressure sensing array (8 by 8) mounted on a balloon catheter, with capabilities in mapping the pressure distributions at tissue interfaces during cardiac surgery.[7] These PU or silicone balloons can deflate during insertion and inflate during surgery. In the deflated state, the sensors collapse together with the balloon to reduce the overall dimensions for minimally invasive insertion. Expansion via inflation allows for interfaces with tissues over large areas (≈1 cm^2). All the materials (i.e., Au, PI, silicone elastomer and others) exploited here are biocompatible, and can be patterned precisely through lithographic techniques. Afterwards, the pressure sensors and other functional components together form a multilayer structure on a balloon catheter through layer-by-layer transfer printing. These features provide means to construct pressure sensor arrays with high spatial resolution for measurements of pressure distributions.

Other biomedical applications of minimally invasive pressure sensors include continuous monitoring of IOP to improve glaucoma management,[276,277] long-term measurement of urinary bladder pressure for the assessment of dysfunction,[278] and pressure monitoring in the aneurysm sac after endovascular repair to prevent endoleak.[279]

3.2.2. Biodegradable Sensors

In some cases, such as monitoring of ICP after a severe traumatic brain injury, the relevant operational time extends only through the critical risk period at the initial stages of recovery. Current practice, therefore, requires a surgical process to remove the devices from the intracranial space, but with additional risks and costs of care. A promising strategy that eliminates this secondary surgery exploits biodegradable sensors, designed to naturally disappear in biofluids after a relevant period of time.[245] Beyond continuous monitoring of pressure for traumatic brain injuries,[84,245,280,281] additional applications are in orthopedic rehabilitation[118] and cardiovascular diseases.[136] Enabling materials include monocrystalline silicon and metal oxides (e.g., ZnO) as semiconductors[282] for piezoresistive or piezoelectric sensing, metals (e.g., Mg, Zn, Mo, W) as conductors for electrodes and interconnects,[118,136,245] and silicon nitride, silicon oxide, and various polymers (e.g., PLGA,[36,124,245,280] poly(L-lactide) (PLLA),[118,136] poly(octamethylene maleate (anhydride) citrate) (POMaC),[118,136] and PHB/PHV,[136] and natural wax) as insulators for dielectrics, substrates and encapsulation structures.[283]

Figure 6B shows an implantable bioresorbable pressure sensor of ICP, capable of chronic operation in vivo for up to 4 weeks.[84] The device consists of a Si substrate (lateral dimension: 1.3 mm by 1.3 mm, thickness: ≈15 μm, dimension of the trench at the center: 200 μm by 200 μm), a thermally grown SiO_2 layer as encapsulation that extends the time for bioresorption (thickness: ≈10 nm), a monocrystalline Si nanomembrane as the resistive material (t-SiO_2, thickness: ≈200 nm, doped with phosphorus at a concentration of ≈1×10^{19} cm^{-3}, GF: −20.9), and a SiO_2 layer formed by electron-beam evaporation (eb-SiO_2, thickness: ≈600 nm). This eb-SiO_2 material separates the conductive Si nanomembrane into four sensors that form a Wheatstone bridge (two strain gauges extend on top of the trench and two temperature gauges directly adhere to the Si substrate). The encapsulation layer of t-SiO_2 allows for stable operation over 25 days with a sensitivity of −0.13 $mmHg^{-1}$. Complete degradation in biofluids occurs over a period of

© 2023 The Authors. Advanced Materials published by Wiley-VCH GmbH

RIGHTSLINK
15214095, 2024, 43, Downloaded from https://onlinelibrary.wiley.com/doi/10.1002/adma.202205609 by Northwestern University Libraries, Wiley Online Library on [25/10/2024]. See the Terms and Conditions (https://onlinelibrary.wiley.com/terms-and-conditions) on Wiley Online Library for rules of use; OA articles are governed by the applicable Creative Commons License

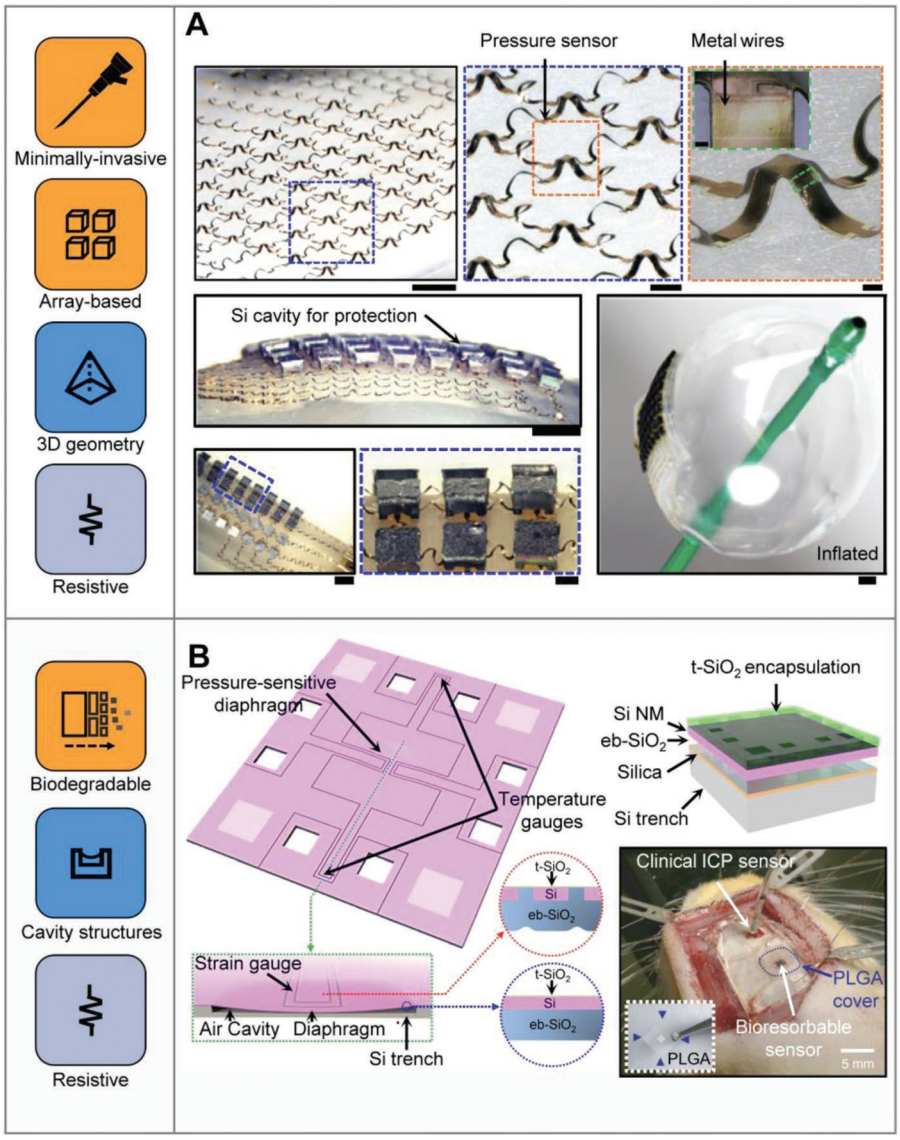

Figure 6. Minimally invasive and bioresorbable bio-interfaced pressure sensors. A) An array of 3D pressure sensors integrated on a balloon catheter for pressure mapping at tissue interfaces during minimally invasive surgery. Scale bars, 2 mm for the images in black outline, 500 µm for images in blue dashed outline, and 100 µm for images in orange dashed outline. Reproduced with permission.[7] Copyright 2020, Springer Nature. B) Bioresorbable pressure sensor for monitoring recovery processes or progression of diseases. Reproduced with permission.[84] Copyright 2018, Springer Nature.

slightly more than a year. The distinct dissolution rates of SiO_2 layers formed by different deposition approaches (i.e., thermally grown and electron-beam evaporation) provide opportunities to control the operational lifetime of such bioresorbable pressure sensors.[283]

Other examples of bioresorbable pressure sensors of ICP include an optical device formed in bioresorbable Si and SiO_2 that exploits Fabry-Perot resonances,[2] and a LRC sensor (PLGA as the membrane, Zn foil integrated in the PLGA membrane as the flexible electrode, and Mg foil etched with a trench as the fixed electrode) that operates remotely through inductive coupling.[245]

A key challenge with such devices is in maintaining stable performance (e.g., the shift in sensitivity, the change in sensing range) during the process of biodegradation by eliminating effects of changes in the properties of the constituent materials. Strategic structural designs and careful selections of materials are critically important. One scheme involves sealing the cavity with bilayers of materials, where the top layer possesses a higher modulus than the bottom layer (e.g., Si as the top layer, PLGA as the bottom layer).[280] Integrating the resistive material inside the bottom layer at a proper position through its thickness allows for sensitivity that does not change as the top layer, exposed to biofluids, degrades. This positioning balances factors that increase and decrease the sensitivity, i.e., the bending stiffness of the bilayer and the distance from the sensing element to the neutral mechanical plane, respectively.

© 2023 The Authors. Advanced Materials published by Wiley-VCH GmbH

RIGHTSLINK

15214095, 2024, 43, Downloaded from https://onlinelibrary.wiley.com/doi/10.1002/adma.202205609 by Northwestern University Libraries, Wiley Online Library on [25/10/2024]. See the Terms and Conditions (https://onlinelibrary.wiley.com/terms-and-conditions) on Wiley Online Library for rules of use; OA articles are governed by the applicable Creative Commons License

4. Conclusion

This review summarizes the metrics, materials and engineered structures associated with emerging classes of pressure sensors, with an emphasis on those with uses in biomedicine. Such devices must balance requirements in high linearity, low hysteresis and drift, fast response time, and stable long-term performance, subject to fundamental constraints set by soft constituent materials and unconventional structural designs. For example, measurements of BP require pressure sensors with fast response times, whereas those monitoring of ICP demand low drift. Bio-interfaced pressure sensors for these and other purposes benefit from low stiffnesses and compliant mechanical properties to facilitate soft, noninvasive and conformal contact with biological tissues. Options include organic materials that have intrinsically low moduli, inorganic materials in ultrathin geometries or 3D architectures and composites that include inorganic nanoparticles or nanowires in polymer matrices. Integrating these materials in structures that enable or amplify out-of-plane deformations is a common design strategy. Examples range from 3D geometries, micropatterns, to meshes, fibers and suspended membranes.

Recent demonstrations of bio-interfaced sensors in continuous monitoring of pressure at the skin interface, in spatiotemporal mapping of pressure distributions on the cardiac surface, and in measurements of internal body processes suggest promise for these technologies in practical applications. Future opportunities lie in the development of i) materials that simultaneously support both high sensitivity, wide dynamic range and excellent stability, ii) manufacturing schemes that can form arrays of sensors at high spatial resolution and/or across large areas, or that can integrate functional circuits and sensors on 3D surfaces,[284] iii) functions beyond pressure that can decouple complex mechanical stimuli (such as shearing, bending, twisting and stretching), or even other parameters[285] (e.g., modulus, proximity, temperature, thermal conductivity, humidity), and iv) devices and systems that can reduce noise to further enhance the signal-to-noise ratio in biomedical measurements.[286,287] Integration of these types of bio-interfaced pressures with other sensor and actuator systems create additional areas for further work. Envisioned possibilities include therapeutic systems with simultaneous, closed-loop capabilities in assessment and remedy, along with adapted versions of these technologies for other fields of use such as those in soft robotics and human–machine interfaces.

Acknowledgements

Z.N. and J.W.K. contributed equally to this work. M.H. acknowledges support from the National Natural Science Foundation of China (grant no. 62104009). J.A.R. acknowledges support from the Querrey-Simpson Institute for Bioelectronics.

Conflict of Interest

The authors declare no conflict of interest.

Keywords

active materials, bio-interfaces, pressure sensors, soft electronics

Received: June 20, 2022
Revised: July 31, 2022
Published online: February 23, 2023

[1] M. W. A. Khan, T. Bjorninen, L. Sydanheimo, L. Ukkonen, *IEEE Microwave Wireless Compon. Lett.* **2016**, *26*, 549.
[2] J. Shin, Z. Liu, W. Bai, Y. Liu, Y. Yan, Y. Xue, I. Kandela, M. Pezhouh, M. R. MacEwan, Y. Huang, W. Z. Ray, W. Zhou, J. A. Rogers, *Sci. Adv.* **2019**, *5*, eaaw1899.
[3] A. Agarwal, A. Shapero, D. Rodger, M. Humayun, Y.-C. Tai, A. Emami, presented at *2018 IEEE Custom Integrated Circuits Conference (CICC)*, San Diego, CA, USA, April **2018**.
[4] F. G. Carrasco, D. D. Alonso, L. Niño-de-Rivera, *Microelectron. Eng.* **2016**, *159*, 32.
[5] C. Schade, A. Phan, K. Joslin, F. E. Talke, *Microsyst. Technol.* **2021**, *27*, 2263.
[6] J. Kim, J. Park, Y. G. Park, E. Cha, M. Ku, H. S. An, K. P. Lee, M. I. Huh, J. Kim, T. S. Kim, D. W. Kim, H. K. Kim, J. U. Park, *Nat. Biomed. Eng.* **2021**, *5*, 772.
[7] M. Han, L. Chen, K. Aras, C. Liang, X. Chen, H. Zhao, K. Li, N. R. Faye, B. Sun, J. H. Kim, W. Bai, Q. Yang, Y. Ma, W. Lu, E. Song, J. M. Baek, Y. Lee, C. Liu, J. B. Model, G. Yang, R. Ghaffari, Y. Huang, I. R. Efimov, J. A. Rogers, *Nat. Biomed. Eng.* **2020**, *4*, 997.
[8] X. Cheng, X. Xue, Y. Ma, M. Han, W. Zhang, Z. Xu, H. Zhang, H. Zhang, *Nano Energy* **2016**, *22*, 453.
[9] N. Luo, W. Dai, C. Li, Z. Zhou, L. Lu, C. C. Poon, S. C. Chen, Y. Zhang, N. Zhao, *Adv. Funct. Mater.* **2016**, *26*, 1178.
[10] K. Meng, J. Chen, X. Li, Y. Wu, W. Fan, Z. Zhou, Q. He, X. Wang, X. Fan, Y. Zhang, *Adv. Funct. Mater.* **2019**, *29*, 1806388.
[11] C.-C. Yeh, S.-H. Lo, M.-X. Xu, Y.-J. Yang, *Microelectron. Eng.* **2019**, *213*, 55.
[12] J. W. Kwak, M. Han, Z. Xie, H. U. Chung, J. Y. Lee, R. Avila, J. Yohay, X. Chen, C. Liang, M. Patel, *Sci. Transl. Med.* **2020**, *12*, eabc4327.
[13] Y. Park, K. Kwon, S. S. Kwak, D. S. Yang, J. W. Kwak, H. Luan, T. S. Chung, K. S. Chun, J. U. Kim, H. Jang, H. Ryu, H. Jeong, S. M. Won, Y. J. Kang, M. Zhang, D. Pontes, B. R. Kampmeier, S. H. Seo, J. Zhao, I. Jung, Y. Huang, S. Xu, J. A. Rogers, *Sci. Adv.* **2020**, *6*, eabe1655.
[14] M. Han, H. Wang, Y. Yang, C. Liang, W. Bai, Z. Yan, H. Li, Y. Xue, X. Wang, B. Akar, *Nat. Electron.* **2019**, *2*, 26.
[15] S. Wang, J. Xu, W. Wang, G. N. Wang, R. Rastak, F. Molina-Lopez, J. W. Chung, S. Niu, V. R. Feig, J. Lopez, T. Lei, S. K. Kwon, Y. Kim, A. M. Foudeh, A. Ehrlich, A. Gasperini, Y. Yun, B. Murmann, J. B. Tok, Z. Bao, *Nature* **2018**, *555*, 83.
[16] Y. Dong, A. N. Ramey-Ward, K. Salaita, *Adv. Mater.* **2021**, *33*, 2006600.
[17] S. Tibbits, *Active Matter*, MIT Press, Cambridge, MA **2017**.
[18] S. R. A. Ruth, V. R. Feig, H. Tran, Z. Bao, *Adv. Funct. Mater.* **2020**, *30*, 2003491.
[19] Y. Chang, L. Wang, R. Li, Z. Zhang, Q. Wang, J. Yang, C. F. Guo, T. Pan, *Adv. Mater.* **2021**, *33*, 2003464.
[20] S. Stassi, V. Cauda, G. Canavese, C. F. Pirri, *Sensors* **2014**, *14*, 5296.
[21] H. Luan, Y. Zhang, *Adv. Intell. Syst.* **2021**, 2000228.
[22] S. Zhang, S. Li, Z. Xia, K. Cai, *J. Mater. Chem. B* **2020**, *8*, 852.
[23] Y. Zang, F. Zhang, C.-a. Di, D. Zhu, *Mater. Horiz.* **2015**, *2*, 140.
[24] J. Li, R. R. Bao, J. Tao, Y. Y. Peng, C. F. Pan, *J. Mater. Chem. C* **2018**, *6*, 11878.
[25] J. Heikenfeld, A. Jajack, J. Rogers, P. Gutruf, L. Tian, T. Pan, R. Li, M. Khine, J. Kim, J. Wang, J. Kim, *Lab Chip* **2018**, *18*, 217.

© 2023 The Authors. Advanced Materials published by Wiley-VCH GmbH

RIGHTSLINK

15214095, 2024, 43, Downloaded from https://onlinelibrary.wiley.com/doi/10.1002/adma.202205609 by Northwestern University Libraries, Wiley Online Library on [25/10/2024]. See the Terms and Conditions (https://onlinelibrary.wiley.com/terms-and-conditions) on Wiley Online Library for rules of use; OA articles are governed by the applicable Creative Commons License

[26] J. C. Yang, J. Mun, S. Y. Kwon, S. Park, Z. N. Bao, S. Park, *Adv. Mater.* **2019**, *31*, 1904765.
[27] T. R. Ray, J. Choi, A. J. Bandodkar, S. Krishnan, P. Gutruf, L. M. Tian, R. Ghaffari, J. A. Rogers, *Chem. Rev.* **2019**, *119*, 5461.
[28] C. M. Boutry, A. Nguyen, Q. O. Lawal, A. Chortos, S. Rondeau-Gagne, Z. Bao, *Adv. Mater.* **2015**, *27*, 6954.
[29] H. Kou, L. Zhang, Q. Tan, G. Liu, H. Dong, W. Zhang, J. Xiong, *Sci. Rep.* **2019**, *9*, 3916.
[30] Q. Liu, Z. Liu, C. Li, K. Xie, P. Zhu, B. Shao, J. Zhang, J. Yang, J. Zhang, Q. Wang, C. F. Guo, *Adv. Sci.* **2020**, *7*, 2000348.
[31] T. Jung, S. Yang, *Sensors* **2015**, *15*, 11823.
[32] J. Wu, Y. Yao, Y. Zhang, T. Shao, H. Wu, S. Liu, Z. Li, L. Wu, *Nanoscale* **2020**, *12*, 21198.
[33] P. Lu, L. Wang, P. Zhu, J. Huang, Y. Wang, N. Bai, Y. Wang, G. Li, J. Yang, K. Xie, J. Zhang, B. Yu, Y. Dai, C. F. Guo, *Sci. Bull.* **2021**, *66*, 1091.
[34] E. O'Brien, J. Petrie, W. Littler, M. de Swiet, P. L. Padfield, D. G. Altman, M. Bland, A. Coats, N. Atkins, *J. Hypertens.* **1993**, *11*, 677.
[35] P. K. Whelton, R. M. Carey, W. S. Aronow, D. E. Casey, K. J. Collins, C. Dennison Himmelfarb, S. M. DePalma, S. Gidding, K. A. Jamerson, D. W. Jones, *J. Am. College Cardiol.* **2018**, *71*, e127.
[36] S. K. Kang, R. K. Murphy, S. W. Hwang, S. M. Lee, D. V. Harburg, N. A. Krueger, J. Shin, P. Gamble, H. Cheng, S. Yu, Z. Liu, J. G. McCall, M. Stephen, H. Ying, J. Kim, G. Park, R. C. Webb, C. H. Lee, S. Chung, D. S. Wie, A. D. Gujar, B. Vemulapalli, A. H. Kim, K. M. Lee, J. Cheng, Y. Huang, S. H. Lee, P. V. Braun, W. Z. Ray, J. A. Rogers, *Nature* **2016**, *530*, 71.
[37] J. Ghajar, *Lancet* **2000**, *356*, 923.
[38] T. Gopesh, A. Camp, M. Unanian, J. Friend, R. N. Weinreb, *Transl. Vis. Sci. Technol.* **2020**, *9*, 28.
[39] J. B. Jonas, N. Wang, Y. X. Wang, Q. S. You, D. Yang, L. Xu, *PLoS One* **2014**, *9*, e100533.
[40] S. Lee, S. Franklin, F. A. Hassani, T. Yokota, M. O. G. Nayeem, Y. Wang, R. Leib, G. Cheng, D. W. Franklin, T. Someya, *Science* **2020**, *370*, 966.
[41] Y.-C. Huang, Y. Liu, C. Ma, H.-C. Cheng, Q. He, H. Wu, C. Wang, C.-Y. Lin, Y. Huang, X. Duan, *Nat. Electron.* **2020**, *3*, 59.
[42] Q. Wang, W. Hong, L. Dong, *Nanoscale* **2016**, *8*, 7663.
[43] P. Lv, J. Qian, C. Yang, T. Liu, Y. Wang, D. Wang, S. Huang, X. Cheng, Z. Cheng, *Nano Energy* **2022**, *97*, 107182.
[44] C. S. Boland, U. Khan, G. Ryan, S. Barwich, R. Charifou, A. Harvey, C. Backes, Z. Li, M. S. Ferreira, M. E. Mobius, R. J. Young, J. N. Coleman, *Science* **2016**, *354*, 1257.
[45] IEEE, *IEEE Standard for Sensor Performance Parameter Definitions*, IEEE Electron Devices Society, New York **2017**.
[46] L. M. Ferson, *Standards and Practices for Instrumentation*, Instrument Society of America, **1980**.
[47] M. Kameda, H. Seki, T. Makoshi, Y. Amao, K. Nakakita, *Sens. Actuators, B* **2012**, *171*, 343.
[48] G. Yu, J. Hu, J. Tan, Y. Gao, Y. Lu, F. Xuan, *Nanotechnology* **2018**, *29*, 115502.
[49] S. L. Passman, *J. Elasticity* **1984**, *14*, 201.
[50] H. T. Banks, *Nonlinear Anal.: Theory, Methods Appl.* **2008**, *69*, 807.
[51] S. C. Mannsfeld, B. C. Tee, R. M. Stoltenberg, C. V. Chen, S. Barman, B. V. Muir, A. N. Sokolov, C. Reese, Z. Bao, *Nat. Mater.* **2010**, *9*, 859.
[52] S. Zhang, C. Ge, R. Liu, *Sens. Actuators, A* **2022**, *341*, 113580.
[53] H. Yao, W. Yang, W. Cheng, Y. J. Tan, H. H. See, S. Li, H. P. A. Ali, B. Z. H. Lim, Z. Liu, B. C. K. Tee, *Proc. Natl. Acad. Sci. USA* **2020**, *117*, 25352.
[54] J. Hwang, S. G. Lee, S. Kim, J. S. Kim, D. H. Kim, W. H. Lee, *ACS Appl. Polym. Mater.* **2020**, *2*, 2190.
[55] J. S. Bergström, M. C. Boyce, *J. Mech. Phys. Solids* **1998**, *46*, 931.
[56] S. Han, J. Kim, S. M. Won, Y. Ma, D. Kang, Z. Xie, K. T. Lee, H. U. Chung, A. Banks, S. Min, S. Y. Heo, C. R. Davies, J. W. Lee, C. H. Lee, B. H. Kim, K. Li, Y. Zhou, C. Wei, X. Feng, Y. Huang, J. A. Rogers, *Sci. Transl. Med.* **2018**, *10*, eaan4950.
[57] S. P. Timoshenko, J. M. Gere, *Theory of Elastic Stability*, Courier Corporation, N. Chelmsford, MA, USA **2009**.
[58] H. T. Zhang, J. Tersoff, S. Xu, H. X. Chen, Q. B. Zhang, K. L. Zhang, Y. Yang, C. S. Lee, K. N. Tu, J. Li, Y. Lu, *Sci. Adv.* **2016**, *2*, e1501382.
[59] S. Wang, Y. Nie, H. Zhu, Y. Xu, S. Cao, J. Zhang, Y. Li, J. Wang, X. Ning, D. Kong, *Sci. Adv.* **2022**, *8*, eabl5511.
[60] G. Suo, Y. Yu, Z. Zhang, S. Wang, P. Zhao, J. Li, X. Wang, *ACS Appl. Mater. Interfaces* **2016**, *8*, 34335.
[61] F. R. Fan, L. Lin, G. Zhu, W. Wu, R. Zhang, Z. L. Wang, *Nano Lett.* **2012**, *12*, 3109.
[62] L. Lin, Y. Xie, S. Wang, W. Wu, S. Niu, X. Wen, Z. L. Wang, *ACS Nano* **2013**, *7*, 8266.
[63] Y. S. Oh, J. H. Kim, Z. Xie, S. Cho, H. Han, S. W. Jeon, M. Park, M. Namkoong, R. Avila, Z. Song, S. U. Lee, K. Ko, J. Lee, J. S. Lee, W. G. Min, B. J. Lee, M. Choi, H. U. Chung, J. Kim, M. Han, J. Koo, Y. S. Choi, S. S. Kwak, S. B. Kim, J. Kim, J. Choi, C. M. Kang, J. U. Kim, K. Kwon, S. M. Won, et al., *Nat. Commun.* **2021**, *12*, 5008.
[64] T. V. Nguyen, Y. Mizuki, T. Tsukagoshi, T. Takahata, M. Ichiki, I. Shimoyama, *Sensors* **2020**, *20*, 1052.
[65] J. Engel, J. Chen, C. Liu, *Appl. Phys. Lett.* **2006**, *89*, 221907.
[66] R. Lakhmi, H. Debeda, I. Dufour, C. Lucat, *IEEE Sens. J.* **2010**, *10*, 1133.
[67] S. M. Won, H. Wang, B. H. Kim, K. Lee, H. Jang, K. Kwon, M. Han, K. E. Crawford, H. Li, Y. Lee, X. Yuan, S. B. Kim, Y. S. Oh, W. J. Jang, J. Y. Lee, S. Han, J. Kim, X. Wang, Z. Xie, Y. Zhang, Y. Huang, J. A. Rogers, *ACS Nano* **2019**, *13*, 10972.
[68] W. Singhatanadgit, *Bone Tissue Regener. Insights* **2009**, *2*, BTRI.S3150.
[69] D. Kang, P. V. Pikhitsa, Y. W. Choi, C. Lee, S. S. Shin, L. Piao, B. Park, K. Y. Suh, T. I. Kim, M. Choi, *Nature* **2014**, *516*, 222.
[70] Y. W. Choi, D. Kang, P. V. Pikhitsa, T. Lee, S. M. Kim, G. Lee, D. Tahk, M. Choi, *Sci. Rep.* **2017**, *7*, 40116.
[71] Y.-L. Park, B.-R. Chen, R. J. Wood, *IEEE Sens. J.* **2012**, *12*, 2711.
[72] D. M. Vogt, Y.-L. Park, R. J. Wood, *IEEE Sens. J.* **2013**, *13*, 4056.
[73] X. Shi, C.-H. Cheng, Y. Zheng, P. K. A. Wai, *J. Micromech. Microeng.* **2016**, *26*, 105020.
[74] J. H. Oh, J. Y. Woo, S. Jo, C.-S. Han, *Sens. Actuators, A* **2019**, *299*, 111610.
[75] K. Kim, J. Choi, Y. Jeong, I. Cho, M. Kim, S. Kim, Y. Oh, I. Park, *Adv. Healthcare Mater.* **2019**, *8*, 1900978.
[76] K. Nan, S. Babaee, W. W. Chan, J. L. P. Kuosmanen, V. R. Feig, Y. Luo, S. S. Srinivasan, C. M. Patterson, A. M. Jebran, G. Traverso, *Nat. Biomed. Eng.* **2022**, *1*, https://doi.org/10.1038/s41551-022-00859-5.
[77] A. Leber, C. Dong, R. Chandran, T. Das Gupta, N. Bartolomei, F. Sorin, *Nat. Electron.* **2020**, *3*, 316.
[78] Y. Ren, X. Sun, J. Liu, *Micromachines* **2020**, *11*, 200.
[79] S. Liu, D. S. Shah, R. Kramer-Bottiglio, *Nat. Mater.* **2021**, *20*, 851.
[80] S. Liu, M. C. Yuen, E. L. White, J. W. Boley, B. Deng, G. J. Cheng, R. Kramer-Bottiglio, *ACS Appl. Mater. Interfaces* **2018**, *10*, 28232.
[81] S. Yang, N. Lu, *Sensors* **2013**, *13*, 8577.
[82] A. A. Barlian, W. T. Park, J. R. Mallon, Jr., A. J. Rastegar, B. L. Pruitt, *Proc. IEEE Inst. Electr. Electron Eng.* **2009**, *97*, 513.
[83] J. Kim, M. Lee, H. J. Shim, R. Ghaffari, H. R. Cho, D. Son, Y. H. Jung, M. Soh, C. Choi, S. Jung, K. Chu, D. Jeon, S. T. Lee, J. H. Kim, S. H. Choi, T. Hyeon, D. H. Kim, *Nat. Commun.* **2014**, *5*, 5747.
[84] J. Shin, Y. Yan, W. Bai, Y. Xue, P. Gamble, L. Tian, I. Kandela, C. R. Haney, W. Spees, Y. Lee, M. Choi, J. Ko, H. Ryu, J. K. Chang, M. Pezhouh, S. K. Kang, S. M. Won, K. J. Yu, J. Zhao, Y. K. Lee, M. R. MacEwan, S. K. Song, Y. Huang, W. Z. Ray, J. A. Rogers, *Nat. Biomed. Eng.* **2019**, *3*, 37.

© 2023 The Authors. Advanced Materials published by Wiley-VCH GmbH

RIGHTSLINK

15214095, 2024, 43, Downloaded from https://onlinelibrary.wiley.com/doi/10.1002/adma.202205609 by Northwestern University Libraries, Wiley Online Library on [25/10/2024]. See the Terms and Conditions (https://onlinelibrary.wiley.com/terms-and-conditions) on Wiley Online Library for rules of use; OA articles are governed by the applicable Creative Commons License

[85] M. Fragaa, H. Furlan, M. Massia, I. Oliveiraa, L. Koberstein, *Proc. Eng.* **2010**, *5*, 609.
[86] B. R. Burg, T. Helbling, C. Hierold, D. Poulikakos, *J. Appl. Phys.* **2011**, *109*, 064310.
[87] R. Yang, Y. Chang, X. Yang, J. Dai, Y. Chen, W. Chang, W. Xiong, *Composites, Part B* **2021**, *217*, 108818.
[88] M. A. Meitl, Z.-T. Zhu, V. Kumar, K. J. Lee, X. Feng, Y. Y. Huang, I. Adesida, R. G. Nuzzo, J. A. Rogers, *Nat. Mater.* **2005**, *5*, 33.
[89] A. Carlson, A. M. Bowen, Y. Huang, R. G. Nuzzo, J. A. Rogers, *Adv. Mater.* **2012**, *24*, 5284.
[90] H. Fang, K. J. Yu, C. Gloschat, Z. Yang, C. H. Chiang, J. Zhao, S. M. Won, S. Xu, M. Trumpis, Y. Zhong, E. Song, S. W. Han, Y. Xue, D. Xu, G. Cauwenberghs, M. Kay, Y. Huang, J. Viventi, I. R. Efimov, J. A. Rogers, *Nat. Biomed. Eng.* **2017**, *1*, 0038.
[91] J. Li, E. Song, C. H. Chiang, K. J. Yu, J. Koo, H. Du, Y. Zhong, M. Hill, C. Wang, J. Zhang, Y. Chen, L. Tian, Y. Zhong, G. Fang, J. Viventi, J. A. Rogers, *Proc. Natl. Acad. Sci. USA* **2018**, *115*, E9542.
[92] H. Jang, W. Lee, S. M. Won, S. Y. Ryu, D. Lee, J. B. Koo, S. D. Ahn, C. W. Yang, M. H. Jo, J. H. Cho, J. A. Rogers, J. H. Ahn, *Nano Lett.* **2013**, *13*, 5600.
[93] D. H. Kim, *Science* **2011**, *333*, 1703.
[94] D. H. Kim, J. Song, W. M. Choi, H. S. Kim, R. H. Kim, Z. Liu, Y. Y. Huang, K. C. Hwang, Y. W. Zhang, J. A. Rogers, *Proc. Natl. Acad. Sci. USA* **2008**, *105*, 18675.
[95] D. Y. Khang, H. Jiang, Y. Huang, J. A. Rogers, *Science* **2006**, *311*, 208.
[96] W. M. Choi, J. Song, D. Y. Khang, H. Jiang, Y. Y. Huang, J. A. Rogers, *Nano Lett.* **2007**, *7*, 1655.
[97] D. Toker, D. Azulay, N. Shimoni, I. Balberg, O. Millo, *Phys. Rev. B* **2003**, *68*, 041403.
[98] L. Shi, Z. Li, M. Chen, Y. Qin, Y. Jiang, L. Wu, *Nat. Commun.* **2020**, *11*, 3529.
[99] M. Chen, W. Luo, Z. Xu, X. Zhang, B. Xie, G. Wang, M. Han, *Nat. Commun.* **2019**, *10*, 4024.
[100] S. Gong, W. Schwalb, Y. Wang, Y. Chen, Y. Tang, J. Si, B. Shirinzadeh, W. Cheng, *Nat. Commun.* **2014**, *5*, 3132.
[101] M. Liu, X. Pu, C. Jiang, T. Liu, X. Huang, L. Chen, C. Du, J. Sun, W. Hu, Z. L. Wang, *Adv. Mater.* **2017**, *29*, 1703700.
[102] S. Jung, J. H. Kim, J. Kim, S. Choi, J. Lee, I. Park, T. Hyeon, D. H. Kim, *Adv. Mater.* **2014**, *26*, 4825.
[103] Y. Liu, L.-Q. Tao, D.-Y. Wang, T.-Y. Zhang, Y. Yang, T.-L. Ren, *Appl. Phys. Lett.* **2017**, *110*, 123508.
[104] Z. Lou, S. Chen, L. Wang, K. Jiang, G. Shen, *Nano Energy* **2016**, *23*, 7.
[105] Y. Wang, Y. Su, Y. Zhang, M. Chen, *ACS Appl. Mater. Interfaces* **2022**, *14*, 5661.
[106] N. Hu, Y. Karube, M. Arai, T. Watanabe, C. Yan, Y. Li, Y. Liu, H. Fukunaga, *Carbon* **2010**, *48*, 680.
[107] S. Chen, X. Guo, *IEEE Trans. Nanotechnol.* **2015**, *14*, 619.
[108] C. Gerlach, D. Krumm, M. Illing, J. Lange, O. Kanoun, S. Odenwald, A. Hubler, *IEEE Sens. J.* **2015**, *15*, 3647.
[109] Z. Wen, J. Yang, H. Ding, W. Zhang, D. Wu, J. Xu, Z. Shi, T. Xu, Y. Tian, X. Li, *J. Mater. Sci.: Mater. Electron.* **2018**, *29*, 20978.
[110] J. Y. Sun, C. Keplinger, G. M. Whitesides, Z. Suo, *Adv. Mater.* **2014**, *26*, 7608.
[111] C. C. Kim, H. H. Lee, K. H. Oh, J. Y. Sun, *Science* **2016**, *353*, 682.
[112] S. Ali, D. Maddipatla, B. B. Narakathu, A. A. Chlaihawi, S. Emamian, F. Janabi, B. J. Bazuin, M. Z. Atashbar, *IEEE Sens. J.* **2019**, *19*, 97.
[113] Y. Zhang, S. Liu, Y. Miao, H. Yang, X. Chen, X. Xiao, Z. Jiang, X. Chen, B. Nie, J. Liu, *ACS Appl. Mater. Interfaces* **2020**, *12*, 27961.
[114] L. Ma, X. Shuai, Y. Hu, X. Liang, P. Zhu, R. Sun, C.-p. Wong, *J. Mater. Chem. C* **2018**, *6*, 13232.
[115] S. Masihi, M. Panahi, D. Maddipatla, A. J. Hanson, A. K. Bose, S. Hajian, V. Palaniappan, B. B. Narakathu, B. J. Bazuin, M. Z. Atashbar, *ACS Sens.* **2021**, *6*, 938.
[116] Z. Luo, J. Chen, Z. Zhu, L. Li, Y. Su, W. Tang, O. M. Omisore, L. Wang, H. Li, *ACS Appl. Mater. Interfaces* **2021**, *13*, 7635.
[117] B. Luo, X. Wang, Y. Wang, L. Li, *J. Mater. Chem. A* **2014**, *2*, 510.
[118] C. M. Boutry, Y. Kaizawa, B. C. Schroeder, A. Chortos, A. Legrand, Z. Wang, J. Chang, P. Fox, Z. Bao, *Nat. Electron.* **2018**, *1*, 314.
[119] J. Lee, H. Kwon, J. Seo, S. Shin, J. H. Koo, C. Pang, S. Son, J. H. Kim, Y. H. Jang, D. E. Kim, T. Lee, *Adv. Mater.* **2015**, *27*, 2433.
[120] Y. Ding, R. Geng, R. Zhu, W. Zhang, W. Wang, Z. Wang, *Smart Mater. Struct.* **2021**, *31*, 025015.
[121] C. M. Boutry, M. Negre, M. Jorda, O. Vardoulis, A. Chortos, O. Khatib, Z. Bao, *Sci. Rob.* **2018**, *3*, eaau6914.
[122] S. R. A. Ruth, L. Beker, H. Tran, V. R. Feig, N. Matsuhisa, Z. Bao, *Adv. Funct. Mater.* **2019**, 1903100.
[123] M.-F. Lin, J. Xiong, J. Wang, K. Parida, P. S. Lee, *Nano Energy* **2018**, *44*, 248.
[124] M. A. U. Khalid, M. Ali, A. M. Soomro, S. W. Kim, H. B. Kim, B.-G. Lee, K. H. Choi, *Sens. Actuators, A* **2019**, *294*, 140.
[125] T. Jin, Y. Pan, G. J. Jeon, H. I. Yeom, S. Zhang, K. W. Paik, S. K. Park, *ACS Appl. Mater. Interfaces* **2020**, *12*, 13348.
[126] B. Nie, S. Xing, J. D. Brandt, T. Pan, *Lab Chip* **2012**, *12*, 1110.
[127] J. Vatamanu, D. Bedrov, *J. Phys. Chem. Lett.* **2015**, *6*, 3594.
[128] B. Nie, R. Li, J. Cao, J. D. Brandt, T. Pan, *Adv. Mater.* **2015**, *27*, 6055.
[129] N. Bai, L. Wang, Q. Wang, J. Deng, Y. Wang, P. Lu, J. Huang, G. Li, Y. Zhang, J. Yang, K. Xie, X. Zhao, C. F. Guo, *Nat. Commun.* **2020**, *11*, 209.
[130] R. Li, Y. Si, Z. Zhu, Y. Guo, Y. Zhang, N. Pan, G. Sun, T. Pan, *Adv. Mater.* **2017**, *29*, 1700253.
[131] S. H. Cho, S. W. Lee, S. Yu, H. Kim, S. Chang, D. Kang, I. Hwang, H. S. Kang, B. Jeong, E. H. Kim, S. M. Cho, K. L. Kim, H. Lee, W. Shim, C. Park, *ACS Appl. Mater. Interfaces* **2017**, *9*, 10128.
[132] Q. Su, X. Huang, K. Lan, T. Xue, W. Gao, Q. Zou, *J. Micromech. Microeng.* **2019**, *30*, 015009.
[133] Z. Qiu, Y. Wan, W. Zhou, J. Yang, J. Yang, J. Huang, J. Zhang, Q. Liu, S. Huang, N. Bai, *Adv. Funct. Mater.* **2018**, *28*, 1802343.
[134] P. Zhu, H. Du, X. Hou, P. Lu, L. Wang, J. Huang, N. Bai, Z. Wu, N. X. Fang, C. F. Guo, *Nat. Commun.* **2021**, *12*, 4731.
[135] L. Y. Chen, B. C. Tee, A. L. Chortos, G. Schwartz, V. Tse, D. J. Lipomi, H. S. Wong, M. V. McConnell, Z. Bao, *Nat. Commun.* **2014**, *5*, 5028.
[136] C. M. Boutry, L. Beker, Y. Kaizawa, C. Vassos, H. Tran, A. C. Hinckley, R. Pfattner, S. Niu, J. Li, J. Claverie, Z. Wang, J. Chang, P. M. Fox, Z. Bao, *Nat. Biomed. Eng.* **2019**, *3*, 47.
[137] P. Eswaran, S. Malarvizhi, *Inter. J. Engin. Techn.* **2013**, *5*, 2734.
[138] S. Park, S. W. Heo, W. Lee, D. Inoue, Z. Jiang, K. Yu, H. Jinno, D. Hashizume, M. Sekino, T. Yokota, K. Fukuda, K. Tajima, T. Someya, *Nature* **2018**, *561*, 516.
[139] Z. L. Wang, *Nano Today* **2010**, *5*, 512.
[140] K. Parida, V. Bhavanasi, V. Kumar, R. Bendi, P. S. Lee, *Nano Res.* **2017**, *10*, 3557.
[141] M. Smith, S. Kar-Narayan, *Int. Mater. Rev.* **2021**, *67*, 65.
[142] M. Xu, H. Kang, L. Guan, H. Li, M. Zhang, *ACS Appl. Mater. Interfaces* **2017**, *9*, 34687.
[143] H. G. Yeo, J. Jung, M. Sim, J. E. Jang, H. Choi, *Sensors* **2020**, *20*, 315.
[144] Y. Yang, H. Pan, G. Xie, Y. Jiang, C. Chen, Y. Su, Y. Wang, H. Tai, *Sens. Actuators, A* **2020**, *301*, 111789.
[145] C. Dagdeviren, Y. Su, P. Joe, R. Yona, Y. Liu, Y. S. Kim, Y. Huang, A. R. Damadoran, J. Xia, L. W. Martin, Y. Huang, J. A. Rogers, *Nat. Commun.* **2014**, *5*, 4496.
[146] Z. L. Wang, *Nano Today* **2010**, *5*, 540.
[147] K.-Y. Shin, J. S. Lee, J. Jang, *Nano Energy* **2016**, *22*, 95.
[148] J. S. Lee, K.-Y. Shin, O. J. Cheong, J. H. Kim, J. Jang, *Sci. Rep.* **2015**, *5*, 7887.
[149] Z. Chen, Z. Wang, X. Li, Y. Lin, N. Luo, M. Long, N. Zhao, J. B. Xu, *ACS Nano* **2017**, *11*, 4507.

© 2023 The Authors. Advanced Materials published by Wiley-VCH GmbH

RIGHTSLINK

15214095, 2024, 43, Downloaded from https://onlinelibrary.wiley.com/doi/10.1002/adma.202205609 by Northwestern University Libraries, Wiley Online Library on [25/10/2024]. See the Terms and Conditions (https://onlinelibrary.wiley.com/terms-and-conditions) on Wiley Online Library for rules of use; OA articles are governed by the applicable Creative Commons License

[150] M. H. Syu, Y. J. Guan, W. C. Lo, Y. K. Fuh, *Nano Energy* **2020**, *76*, 105029.
[151] G. Wang, T. Liu, X.-C. Sun, P. Li, Y.-S. Xu, J.-G. Hua, Y.-H. Yu, S.-X. Li, Y.-Z. Dai, X.-Y. Song, *Sens. Actuators, A* **2018**, *280*, 319.
[152] L. Persano, C. Dagdeviren, Y. Su, Y. Zhang, S. Girardo, D. Pisignano, Y. Huang, J. A. Rogers, *Nat. Commun.* **2013**, *4*, 1633.
[153] T. Sharma, S.-S. Je, B. Gill, J. X. Zhang, *Sens. Actuators, A* **2012**, *177*, 87.
[154] W. Guo, C. Tan, K. Shi, J. Li, X.-X. Wang, B. Sun, X. Huang, Y.-Z. Long, P. Jiang, *Nanoscale* **2018**, *10*, 17751.
[155] N. Chamankar, R. Khajavi, A. A. Yousefi, A. Rashidi, F. Golestanifard, *Ceram. Int.* **2020**, *46*, 19669.
[156] Y. Chen, Y. Zhang, F. Yuan, F. Ding, O. G. Schmidt, *Adv. Electron. Mater.* **2017**, *3*, 1600540.
[157] H. Kim, Y. Tadesse, S. Priya, *Energy Harvesting Technologies*, Springer, Berlin, Germany **2009**, p. 3.
[158] C. Dagdeviren, F. Javid, P. Joe, T. von Erlach, T. Bensel, Z. Wei, S. Saxton, C. Cleveland, L. Booth, S. McDonnell, J. Collins, A. Hayward, R. Langer, G. Traverso, *Nat. Biomed. Eng.* **2017**, *1*, 807.
[159] A. Kim, C. R. Powell, B. Ziaie, *IEEE Trans. Biomed. Eng.* **2014**, *61*, 2209.
[160] K. S. Ramadan, D. Sameoto, S. Evoy, *Smart Mater. Struct.* **2014**, *23*, 033001.
[161] J. H. Lee, H. J. Yoon, T. Y. Kim, M. K. Gupta, J. H. Lee, W. Seung, H. Ryu, S. W. Kim, *Adv. Funct. Mater.* **2015**, *25*, 3203.
[162] R. Agrawal, B. Peng, H. D. Espinosa, *Nano Lett.* **2009**, *9*, 4177.
[163] L. Wang, W. Dou, J. Chen, K. Lu, F. Zhang, M. Abdulaziz, W. Su, A. Li, C. Xu, Y. Sun, *Mater. Sci. Eng. C: Mater. Biol. Appl.* **2020**, *117*, 111345.
[164] R. E. Newnham, D. P. Skinner, L. E. Cross, *Mater. Res. Bull.* **1978**, *13*, 525.
[165] I. Babu, G. de With, *Compos. Sci. Technol.* **2014**, *91*, 91.
[166] K. K. Sappati, S. Bhadra, *IEEE Sens. J.* **2020**, *20*, 4610.
[167] D. Liu, Q. Yue, J. Deng, D. Lin, X. Li, W. Di, X. Wang, X. Zhao, H. Luo, *Sensors* **2015**, *15*, 6807.
[168] S. Yi, W. Zhang, G. Gao, H. Xu, D. Xu, *Ceram. Int.* **2018**, *44*, 10940.
[169] P. Wang, L. Hao, Z. Wang, Y. Wang, M. Guo, P. Zhang, *ACS Appl. Mater. Interfaces* **2020**, *12*, 49464.
[170] M. Varga, J. Morvan, N. Diorio, E. Buyuktanir, J. Harden, J. L. West, A. Jákli, *Appl. Phys. Lett.* **2013**, *102*, 153903.
[171] C. T. Pan, Z. H. Liu, Y. C. Chen, C. F. Liu, *Sens. Actuators, A* **2010**, *159*, 96.
[172] Y. Su, C. Dagdeviren, R. Li, *Adv. Funct. Mater.* **2015**, *25*, 5320.
[173] F.-R. Fan, Z.-Q. Tian, Z. L. Wang, *Nano Energy* **2012**, *1*, 328.
[174] M. Ha, S. Lim, S. Cho, Y. Lee, S. Na, C. Baig, H. Ko, *ACS Nano* **2018**, *12*, 3964.
[175] Y. Lee, J. Kim, B. Jang, S. Kim, B. K. Sharma, J.-H. Kim, J.-H. Ahn, *Nano Energy* **2019**, *62*, 259.
[176] H. Zou, Y. Zhang, L. Guo, P. Wang, X. He, G. Dai, H. Zheng, C. Chen, A. C. Wang, C. Xu, Z. L. Wang, *Nat. Commun.* **2019**, *10*, 1427.
[177] Z. You, S. Wang, Z. Li, Y. Zou, T. Lu, F. Wang, B. Hu, X. Wang, L. Li, W. Fang, Y. Liu, *Nano Energy* **2022**, *91*, 106667.
[178] K. Xia, D. Wu, J. Fu, N. A. Hoque, Y. Ye, Z. Xu, *J. Mater. Chem. A* **2020**, *8*, 25995.
[179] Z. Zhang, D. Jiang, J. Zhao, G. Liu, T. Bu, C. Zhang, Z. L. Wang, *Adv. Energy Mater.* **2020**, *10*, 1903713.
[180] L. Pan, J. Wang, P. Wang, R. Gao, Y.-C. Wang, X. Zhang, J.-J. Zou, Z. L. Wang, *Nano Res.* **2018**, *11*, 4062.
[181] P. Jiang, L. Zhang, H. Guo, C. Chen, C. Wu, S. Zhang, Z. L. Wang, *Adv. Mater.* **2019**, *31*, 1902793.
[182] S. Pan, Z. Zhang, *Friction* **2018**, *7*, 2.
[183] S. Liu, W. Zheng, B. Yang, X. Tao, *Nano Energy* **2018**, *53*, 383.
[184] J. Huang, X. Fu, G. Liu, S. Xu, X. Li, C. Zhang, L. Jiang, *Nano Energy* **2019**, *62*, 638.
[185] H. Cho, S. Jo, I. Kim, D. Kim, *ACS Appl. Mater. Interfaces* **2021**, *13*, 48281.
[186] Y. J. Zou, J. Xu, K. Chen, J. Chen, *Adv. Mater. Technol.* **2021**, *6*, 2000916.
[187] C. X. Lu, C. B. Han, G. Q. Gu, J. Chen, Z. W. Yang, T. Jiang, C. He, Z. L. Wang, *Adv. Eng. Mater.* **2017**, *19*, 1700275.
[188] V. Nguyen, R. Yang, *Nano Energy* **2013**, *2*, 604.
[189] M. M. Apodaca, P. J. Wesson, K. J. Bishop, M. A. Ratner, B. A. Grzybowski, *Angew. Chem. Int., Ed. Engl.* **2010**, *49*, 946.
[190] J. Yang, J. Chen, Y. Su, Q. Jing, Z. Li, F. Yi, X. Wen, Z. Wang, Z. L. Wang, *Adv. Mater.* **2015**, *27*, 1316.
[191] H. Lei, Y. F. Chen, Z. Q. Gao, Z. Wen, X. H. Sun, *J. Mater. Chem. A* **2021**, *9*, 20100.
[192] X. Zhao, G. Chen, Y. Zhou, A. Nashalian, J. Xu, T. Tat, Y. Song, A. Libanori, S. Xu, S. Li, J. Chen, *ACS Nano* **2022**, *16*, 6013.
[193] X. Zhao, Y. Zhou, J. Xu, G. Chen, Y. Fang, T. Tat, X. Xiao, Y. Song, S. Li, J. Chen, *Nat. Commun.* **2021**, *12*, 6755.
[194] Y. Zhou, X. Zhao, J. Xu, Y. Fang, G. Chen, Y. Song, S. Li, J. Chen, *Nat. Mater.* **2021**, *20*, 1670.
[195] Y. Yan, Z. Hu, Z. Yang, W. Yuan, C. Song, J. Pan, Y. Shen, *Sci. Rob.* **2021**, *6*, eabc8801.
[196] C. Becker, B. Bao, D. D. Karnaushenko, V. K. Bandari, B. Rivkin, Z. Li, M. Faghih, D. Karnaushenko, O. G. Schmidt, *Nat. Commun.* **2022**, *13*, 2121.
[197] H. Bai, S. Li, J. Barreiros, Y. Tu, C. R. Pollock, R. F. Shepherd, *Science* **2020**, *370*, 848.
[198] L. Massari, G. Fransvea, J. D'Abbraccio, M. Filosa, G. Terruso, A. Aliperta, G. D'Alesio, M. Zaltieri, E. Schena, E. Palermo, *Nat. Mach. Intell.* **2022**, *4*, 425.
[199] L. Lu, N. Zhao, J. Liu, B. Yang, *J. Mater. Chem. C* **2021**, *9*, 9309.
[200] S. Chun, J.-S. Kim, Y. Yoo, Y. Choi, S. J. Jung, D. Jang, G. Lee, K.-I. Song, K. S. Nam, I. Youn, *Nat. Electron.* **2021**, *4*, 429.
[201] K. H. Ha, W. Zhang, H. Jang, S. Kang, L. Wang, P. Tan, H. Hwang, N. Lu, *Adv. Mater.* **2021**, *33*, 2103320.
[202] K. Park, H. Yuk, M. Yang, J. Cho, H. Lee, J. Kim, *Sci. Rob.* **2022**, *7*, eabm7187.
[203] M. Sohgawa, Y. M. Huang, K. Yamashita, T. Kanashima, M. Noda, M. Okuyama, H. Noma, IEEE, presented at *14th International Conference on Solid-State Sensors, Actuators and Microsystems/21st European Conference on Solid-State Transducers*, Lyon, France, Jun 10–14, **2007**.
[204] R. M. R. Pinto, V. Chu, J. P. Conde, *Adv. Eng. Mater.* **2019**, *21*.
[205] S. Xu, Z. Yan, K. I. Jang, W. Huang, H. Fu, J. Kim, Z. Wei, M. Flavin, J. McCracken, R. Wang, A. Badea, Y. Liu, D. Xiao, G. Zhou, J. Lee, H. U. Chung, H. Cheng, W. Ren, A. Banks, X. Li, U. Paik, R. G. Nuzzo, Y. Huang, Y. Zhang, J. A. Rogers, *Science* **2015**, *347*, 154.
[206] G. Peng, W. Fang, J. Lin, *IEEE Trans. Magn.* **1999**, *35*, 3004.
[207] M. Sohgawa, T. Mima, H. Onishi, T. Kanashima, M. Okuyama, K. Yamashita, M. Noda, M. Higuchi, H. Noma, presented at *Transducers 2009-2009 International Solid-State Sensors, Actuators and Microsystems Conference*, Denver, CO, USA, June **2009**.
[208] Z. Yan, F. Zhang, J. Wang, F. Liu, X. Guo, K. Nan, Q. Lin, M. Gao, D. Xiao, Y. Shi, Y. Qiu, H. Luan, J. H. Kim, Y. Wang, H. Luo, M. Han, Y. Huang, Y. Zhang, J. A. Rogers, *Adv. Funct. Mater.* **2016**, *26*, 2629.
[209] Z. Yan, F. Zhang, F. Liu, M. Han, D. Ou, Y. Liu, Q. Lin, X. Guo, H. Fu, Z. Xie, M. Gao, Y. Huang, J. Kim, Y. Qiu, K. Nan, J. Kim, P. Gutruf, H. Luo, A. Zhao, K. C. Hwang, Y. Huang, Y. Zhang, J. A. Rogers, *Sci. Adv.* **2016**, *2*, e1601014.
[210] Y. Zhang, Z. Yan, K. Nan, D. Xiao, Y. Liu, H. Luan, H. Fu, X. Wang, Q. Yang, J. Wang, W. Ren, H. Si, F. Liu, L. Yang, H. Li, J. Wang, X. Guo, H. Luo, L. Wang, Y. Huang, J. A. Rogers, *Proc. Natl. Acad. Sci. USA* **2015**, *112*, 11757.
[211] H. Zhao, K. Li, M. Han, F. Zhu, A. Vazquez-Guardado, P. Guo, Z. Xie, Y. Park, L. Chen, X. Wang, H. Luan, Y. Yang, H. Wang, C. Liang, Y. Xue, R. D. Schaller, D. Chanda, Y. Huang, Y. Zhang, J. A. Rogers, *Proc. Natl. Acad. Sci. USA* **2019**, *116*, 13239.

© 2023 The Authors. Advanced Materials published by Wiley-VCH GmbH

RIGHTSLINK
15214095, 2024, 43, Downloaded from https://onlinelibrary.wiley.com/doi/10.1002/adma.202205609 by Northwestern University Libraries, Wiley Online Library on [25/10/2024]. See the Terms and Conditions (https://onlinelibrary.wiley.com/terms-and-conditions) on Wiley Online Library for rules of use; OA articles are governed by the applicable Creative Commons License

[212] W. Lee, Y. Liu, Y. Lee, B. K. Sharma, S. M. Shinde, S. D. Kim, K. Nan, Z. Yan, M. Han, Y. Huang, Y. Zhang, J. H. Ahn, J. A. Rogers, *Nat. Commun.* **2018**, *9*, 1417.
[213] J. Ye, F. Zhang, Z. Shen, S. Cao, T. Jin, X. Guo, Z. Li, L. Lin, Y. Zhang, *npj Flexible Electron.* **2021**, *5*, 28.
[214] Z. Wang, L. Zhang, J. Liu, H. Jiang, C. Li, *Nanoscale* **2018**, *10*, 10691.
[215] J. Park, Y. Lee, J. Hong, M. Ha, Y. D. Jung, H. Lim, S. Y. Kim, H. Ko, *ACS Nano* **2014**, *8*, 4689.
[216] X. Tian, P. M. Lee, Y. J. Tan, T. L. Wu, H. Yao, M. Zhang, Z. Li, K. A. Ng, B. C. Tee, J. S. Ho, *Nat. Electron.* **2019**, *2*, 243.
[217] W. W. Lee, Y. J. Tan, H. Yao, S. Li, H. H. See, M. Hon, K. A. Ng, B. Xiong, J. S. Ho, B. C. K. Tee, *Sci. Rob.* **2019**, *4*, eaax2198.
[218] A. Chhetry, J. Kim, H. Yoon, J. Y. Park, *ACS Appl. Mater. Interfaces* **2018**, *11*, 3438.
[219] S. R. A. Ruth, Z. Bao, *ACS Appl. Mater. Interfaces* **2020**, *12*, 58301.
[220] J. Qin, L. J. Yin, Y. N. Hao, S. L. Zhong, D. L. Zhang, K. Bi, Y. X. Zhang, Y. Zhao, Z. M. Dang, *Adv. Mater.* **2021**, *33*, 2008267.
[221] T. Zhao, T. Li, L. Chen, L. Yuan, X. Li, J. Zhang, *ACS Appl. Mater. Interfaces* **2019**, *11*, 29466.
[222] Y. Gao, H. Ota, E. W. Schaler, K. Chen, A. Zhao, W. Gao, H. M. Fahad, Y. Leng, A. Zheng, F. Xiong, C. Zhang, L. C. Tai, P. Zhao, R. S. Fearing, A. Javey, *Adv. Mater.* **2017**, *29*, 1701985.
[223] Y. Pang, K. Zhang, Z. Yang, S. Jiang, Z. Ju, Y. Li, X. Wang, D. Wang, M. Jian, Y. Zhang, R. Liang, H. Tian, Y. Yang, T. L. Ren, *ACS Nano* **2018**, *12*, 2346.
[224] C. Pang, G.-Y. Lee, T.-i. Kim, S. M. Kim, H. N. Kim, S.-H. Ahn, K.-Y. Suh, *Nat. Mater.* **2012**, *11*, 795.
[225] L. Pan, A. Chortos, G. Yu, Y. Wang, S. Isaacson, R. Allen, Y. Shi, R. Dauskardt, Z. Bao, *Nat. Commun.* **2014**, *5*, 3002.
[226] T. Yang, H. Xiang, C. Qin, Y. Liu, X. Zhao, H. Liu, H. Li, M. Ouzounian, G. Hong, H. Chen, *Adv. Electron. Mater.* **2020**, *6*, 1900916.
[227] C. L. Choong, M. B. Shim, B. S. Lee, S. Jeon, D. S. Ko, T. H. Kang, J. Bae, S. H. Lee, K. E. Byun, J. Im, *Adv. Mater.* **2014**, *26*, 3451.
[228] Y. Cao, T. Li, Y. Gu, H. Luo, S. Wang, T. Zhang, *Small* **2018**, *14*, 1703902.
[229] H. H. Chou, A. Nguyen, A. Chortos, J. W. To, C. Lu, J. Mei, T. Kurosawa, W. G. Bae, J. B. Tok, Z. Bao, *Nat. Commun.* **2015**, *6*, 8011.
[230] W. Choi, J. Lee, Y. Kyoung Yoo, S. Kang, J. Kim, J. Hoon Lee, *Appl. Phys. Lett.* **2014**, *104*, 123701.
[231] C. Creton, *Macromolecules* **2017**, *50*, 8297.
[232] A. Miyamoto, S. Lee, N. F. Cooray, S. Lee, M. Mori, N. Matsuhisa, H. Jin, L. Yoda, T. Yokota, A. Itoh, M. Sekino, H. Kawasaki, T. Ebihara, M. Amagai, T. Someya, *Nat. Nanotechnol.* **2017**, *12*, 907.
[233] W. Yan, G. Noel, G. Loke, E. Meiklejohn, T. Khudiyev, J. Marion, G. Rui, J. Lin, J. Cherston, A. Sahasrabudhe, J. Wilbert, I. Wicaksono, R. W. Hoyt, A. Missakian, L. Zhu, C. Ma, J. Joannopoulos, Y. Fink, *Nature* **2022**, *603*, 616.
[234] H. D. Liu, H. J. Zhang, W. Q. Han, H. J. Lin, R. Z. Li, J. X. Zhu, W. Huang, *Adv. Mater.* **2021**, *33*, 2004782.
[235] X. Zhou, P. S. Lee, *MRS Bull.* **2021**, *46*, 330.
[236] Q. Zou, Z. Ma, S. Li, Z. Lei, Q. Su, *Sens. Actuators, A* **2020**, *308*, 112012.
[237] S. Lee, A. Reuveny, J. Reeder, S. Lee, H. Jin, Q. Liu, T. Yokota, T. Sekitani, T. Isoyama, Y. Abe, Z. Suo, T. Someya, *Nat. Nanotechnol.* **2016**, *11*, 472.
[238] O. Atalay, A. Atalay, J. Gafford, C. Walsh, *Adv. Mater. Technol.* **2018**, *3*, 1700237.
[239] Y. Cheng, R. Wang, H. Zhai, J. Sun, *Nanoscale* **2017**, *9*, 3834.
[240] K. Dong, Z. Wu, J. Deng, A. C. Wang, H. Zou, C. Chen, D. Hu, B. Gu, B. Sun, Z. L. Wang, *Adv. Mater.* **2018**, *30*, 1804944.
[241] B. Sun, R. N. McCay, S. Goswami, Y. Xu, C. Zhang, Y. Ling, J. Lin, Z. Yan, *Adv. Mater.* **2018**, *30*, 1804327.
[242] Z. Zhu, R. Li, T. Pan, *Adv. Mater.* **2018**, *30*, 1705122.
[243] J. Gafford, Y. Ding, A. Harris, T. McKenna, P. Polygerinos, D. Holland, A. Moser, C. Walsh, *J. Med. Dev.* **2014**, *8*, 030927.
[244] L. P. Jentoft, Y. Tenzer, D. Vogt, J. Liu, R. J. Wood, R. D. Howe, IEEE, presented at *16th International Conference on Advanced Robotics (ICAR)*, Univ Republica, Montevideo, Uruguay, November 25–29, **2013**.
[245] D. Lu, Y. Yan, Y. Deng, Q. Yang, J. Zhao, M. H. Seo, W. Bai, M. R. MacEwan, Y. Huang, W. Z. Ray, J. A. Rogers, *Adv. Funct. Mater.* **2020**, *30*, 2003754.
[246] M. Chattopadhyay, D. Chowdhury, *Microsyst. Technol.* **2016**, *23*, 4203.
[247] W. Chien-Hung, C. A. Zorman, M. Mehregany, *IEEE Sens. J.* **2006**, *6*, 316.
[248] O. Akar, T. Akin, K. Najafi, *Sens. Actuators, A* **2001**, *95*, 29.
[249] Y. Cao, Y. J. Tan, S. Li, W. W. Lee, H. Guo, Y. Cai, C. Wang, B. C.-K. Tee, *Nat. Electron.* **2019**, *2*, 75.
[250] Y. Dobashi, D. Yao, Y. Petel, T. N. Nguyen, M. S. Sarwar, Y. Thabet, C. L. W. Ng, E. Scabeni Glitz, G. T. M. Nguyen, C. Plesse, F. Vidal, C. A. Michal, J. D. W. Madden, *Science* **2022**, *376*, 502.
[251] I. You, D. G. Mackanic, N. Matsuhisa, J. Kang, J. Kwon, L. Beker, J. Mun, W. Suh, T. Y. Kim, J. B. Tok, Z. Bao, U. Jeong, *Science* **2020**, *370*, 961.
[252] G. Li, S. Liu, L. Wang, R. Zhu, *Sci. Rob.* **2020**, *5*, eabc8134.
[253] K. Hickle, R. Slamin, A. Baez, D. Sen, E. Evan-Browning, H. Tessier, Y. Mendelson, J. McNeill, R. Dunn, *Ann. Plast. Surg.* **2019**, *82*, S215.
[254] C. Wang, X. Li, H. Hu, L. Zhang, Z. Huang, M. Lin, Z. Zhang, Z. Yin, B. Huang, H. Gong, S. Bhaskaran, Y. Gu, M. Makihata, Y. Guo, Y. Lei, Y. Chen, C. Wang, Y. Li, T. Zhang, Z. Chen, A. P. Pisano, L. Zhang, Q. Zhou, S. Xu, *Nat. Biomed. Eng.* **2018**, *2*, 687.
[255] S. Li, Y. Park, H. Luan, H. Wang, K. Kwon, J. A. Rogers, Y. Huang, *J. Appl. Mech.* **2021**, *88*, 101008.
[256] X. Wang, Y. Gu, Z. Xiong, Z. Cui, T. Zhang, *Adv. Mater.* **2014**, *26*, 1336.
[257] B. Nie, R. Huang, T. Yao, Y. Zhang, Y. Miao, C. Liu, J. Liu, X. Chen, *Adv. Funct. Mater.* **2019**, *29*, 1808786.
[258] M. G. Allen, IEEE, presented at *13th International Conference on Solid-State Sensors, Actuators and Microsystems*, Seoul, South Korea, June 05–09, **2005**.
[259] S. Honda, Q. Zhu, S. Satoh, T. Arie, S. Akita, K. Takei, *Adv. Funct. Mater.* **2019**, *29*, 1807957.
[260] S. Sundaram, P. Kellnhofer, Y. Li, J.-Y. Zhu, A. Torralba, W. Matusik, *Nature* **2019**, *569*, 698.
[261] R. Lazzarini, R. Magni, P. Dario, presented at Proceedings 1995 IEEE/RSJ International Conference on Intelligent Robots and Systems. Human Robot Interaction and Cooperative Robots, Pittsburgh, PA, USA, August **1995**.
[262] R. C. Webb, A. P. Bonifas, A. Behnaz, Y. Zhang, K. J. Yu, H. Cheng, M. Shi, Z. Bian, Z. Liu, Y. S. Kim, W. H. Yeo, J. S. Park, J. Song, Y. Li, Y. Huang, A. M. Gorbach, J. A. Rogers, *Nat. Mater.* **2013**, *12*, 938.
[263] M. Kondo, M. Melzer, D. Karnaushenko, T. Uemura, S. Yoshimoto, M. Akiyama, Y. Noda, T. Araki, O. G. Schmidt, T. Sekitani, *Sci. Adv.* **2020**, *6*, eaay6094.
[264] M. Park, M.-S. Kim, Y.-K. Park, J.-H. Ahn, *Appl. Phys. Lett.* **2015**, *106*, 043502.
[265] H. Shim, K. Sim, F. Ershad, P. Yang, A. Thukral, Z. Rao, H. J. Kim, Y. Liu, X. Wang, G. Gu, L. Gao, X. Wang, Y. Chai, C. Yu, *Sci. Adv.* **2019**, *5*, eaax4961.
[266] J. Melgaard, N. Rijkhoff, *IEEE Trans. Neural Syst. Rehabil. Eng.* **2011**, *19*, 700.
[267] J. Park, J.-K. Kim, D.-S. Kim, A. Shanmugasundaram, S. A. Park, S. Kang, S.-H. Kim, M. H. Jeong, D.-W. Lee, *Sens. Actuators, B* **2019**, *280*, 201.
[268] H. Fang, J. Zhao, K. J. Yu, E. Song, A. B. Farimani, C.-H. Chiang, X. Jin, Y. Xue, D. Xu, W. Du, *Proc. Natl. Acad. Sci. USA* **2016**, *113*, 11682.

© 2023 The Authors. Advanced Materials published by Wiley-VCH GmbH

RIGHTSLINK
15214095, 2024, 43, Downloaded from https://onlinelibrary.wiley.com/doi/10.1002/adma.202205609 by Northwestern University Libraries, Wiley Online Library on [25/10/2024]. See the Terms and Conditions (https://onlinelibrary.wiley.com/terms-and-conditions) on Wiley Online Library for rules of use; OA articles are governed by the applicable Creative Commons License

[269] D. O'brien, J. White, M. Fonseca, J. Kroh, M. Allen, D. Stern, *Google Patents*, **2005**.
[270] D. H. Kim, N. Lu, R. Ghaffari, Y. S. Kim, S. P. Lee, L. Xu, J. Wu, R. H. Kim, J. Song, Z. Liu, J. Viventi, B. de Graff, B. Elolampi, M. Mansour, M. J. Slepian, S. Hwang, J. D. Moss, S. M. Won, Y. Huang, B. Litt, J. A. Rogers, *Nat. Mater.* **2011**, *10*, 316.
[271] Z. Liu, Y. Ma, H. Ouyang, B. Shi, N. Li, D. Jiang, F. Xie, D. Qu, Y. Zou, Y. Huang, H. Li, C. Zhao, P. Tan, M. Yu, Y. Fan, H. Zhang, Z. L. Wang, Z. Li, *Adv. Funct. Mater.* **2019**, *29*, 1807560.
[272] V. Arabagi, O. Felfoul, A. H. Gosline, R. J. Wood, P. E. Dupont, *IEEE Sens. J.* **2016**, *16*, 1294.
[273] P. J. Codd, A. Veaceslav, A. H. Gosline, P. E. Dupont, *J. Neurosurg. Pediatr.* **2014**, *13*, 114.
[274] J. Park, J. K. Kim, S. J. Patil, J. K. Park, S. Park, D. W. Lee, *Sensors* **2016**, *16*, 809.
[275] E. Y. Chow, A. L. Chlebowski, S. Chakraborty, W. J. Chappell, P. P. Irazoqui, *IEEE Trans. Biomed. Eng.* **2010**, *57*, 1487.
[276] I. Sanchez, R. Martin, *J. Optom.* **2019**, *12*, 211.
[277] G. Chitnis, T. Maleki, B. Samuels, L. B. Cantor, B. Ziaie, *IEEE Trans. Biomed. Eng.* **2013**, *60*, 250.
[278] I. Clausen, W. T. LG, T. Glott, *Sensors* **2018**, *18*.
[279] F. Springer, R. W. Gunther, T. Schmitz-Rode, *Cardiovasc. Interventional Radiol.* **2008**, *31*, 460.
[280] Q. Yang, S. Lee, Y. Xue, Y. Yan, T. L. Liu, S. K. Kang, Y. J. Lee, S. H. Lee, M. H. Seo, D. Lu, *Adv. Funct. Mater.* **2020**, *30*, 1910718.
[281] X. Chen, Y. J. Park, M. Kang, S.-K. Kang, J. Koo, S. M. Shinde, J. Shin, S. Jeon, G. Park, Y. Yan, *Nat. Commun.* **2018**, *9*, 1690.
[282] S. K. Kang, S. W. Hwang, S. Yu, J. H. Seo, E. A. Corbin, J. Shin, D. S. Wie, R. Bashir, Z. Ma, J. A. Rogers, *Adv. Funct. Mater.* **2015**, *25*, 1789.
[283] S. K. Kang, S. W. Hwang, H. Cheng, S. Yu, B. H. Kim, J. H. Kim, Y. Huang, J. A. Rogers, *Adv. Funct. Mater.* **2014**, *24*, 4427.
[284] N. Yi, Y. Y. Gao, A. Lo Verso, J. Zhu, D. Erdely, C. L. Xue, R. Lavelle, H. Y. Cheng, *Mater. Today* **2021**, *50*, 24.
[285] R. X. Yang, W. Q. Zhang, N. Tiwari, H. Yan, T. J. Li, H. Y. Cheng, *Adv. Sci.* **2022**, 2202470, https://doi.org/10.1002/advs.202202470.
[286] B. Park, J. H. Shin, J. Ok, S. Park, W. Jung, C. Jeong, S. Choy, Y. J. Jo, T. I. Kim, *Science* **2022**, *376*, 624.
[287] C. Jeong, J. S. Lee, B. Park, C. S. Hong, J. U. Kim, T. I. Kim, *Adv. Mater.* **2019**, *31*, 1902689.

Zhongyi Nie received his B.S. degree in biomedical engineering from Beihang University in 2022. He is currently a Ph.D. candidate of biomedical engineering at Peking University. His undergraduate and Ph.D. research emphases are on MEMS sensors, flexible electronics, biomedical electronics, implanted electronics, and their translation in clinical applications.

Jean Won Kwak received her B.S. in mechanical engineering with a minor in electrical engineering from the University of Illinois at Urbana-Champaign in 2017. She completed her Ph.D. at Northwestern University in 2021, studying mechanical engineering. Her Ph.D. studies focused on clinical-grade, soft, thin, and flexible miniaturized 3D sensors for wireless skin health monitoring, with an emphasis on pressure sensors. Dr. Kwak is currently a postdoctoral scholar in Radiology at Stanford University.

© 2023 The Authors. Advanced Materials published by Wiley-VCH GmbH

RIGHTSLINK

15214095, 2024, 43, Downloaded from https://onlinelibrary.wiley.com/doi/10.1002/adma.202205609 by Northwestern University Libraries, Wiley Online Library on [25/10/2024]. See the Terms and Conditions (https://onlinelibrary.wiley.com/terms-and-conditions) on Wiley Online Library for rules of use; OA articles are governed by the applicable Creative Commons License

John A. Rogers obtained B.A. and B.S. degrees in chemistry and in physics from the University of Texas, Austin, in 1989. From MIT, he received S.M. degrees in physics and in chemistry in 1992 and a Ph.D. in physical chemistry in 1995. He spent thirteen years on the faculty at University of Illinois, most recently as the Swanlund Chair Professor and Director of the Seitz Materials Research Laboratory. In 2016, he joined Northwestern University as the Louis Simpson and Kimberly Querrey Professor of Materials Science and Engineering, Biomedical Engineering and Neurological Surgery, with affiliate appointments in Mechanical Engineering, Electrical and Computer Engineering, Chemistry and Dermatology.

© 2023 The Authors. Advanced Materials published by Wiley-VCH GmbH

RIGHTSLINK

15214095, 2024, 43, Downloaded from https://onlinelibrary.wiley.com/doi/10.1002/adma.202205609 by Northwestern University Libraries, Wiley Online Library on [25/10/2024]. See the Terms and Conditions (https://onlinelibrary.wiley.com/terms-and-conditions) on Wiley Online Library for rules of use; OA articles are governed by the applicable Creative Commons License